iScience

CellPress
OPEN ACCESS

Article

Natural γδT17 cell development and functional acquisition is governed by the mTORC2-c-Maf-controlled mitochondrial fission pathway

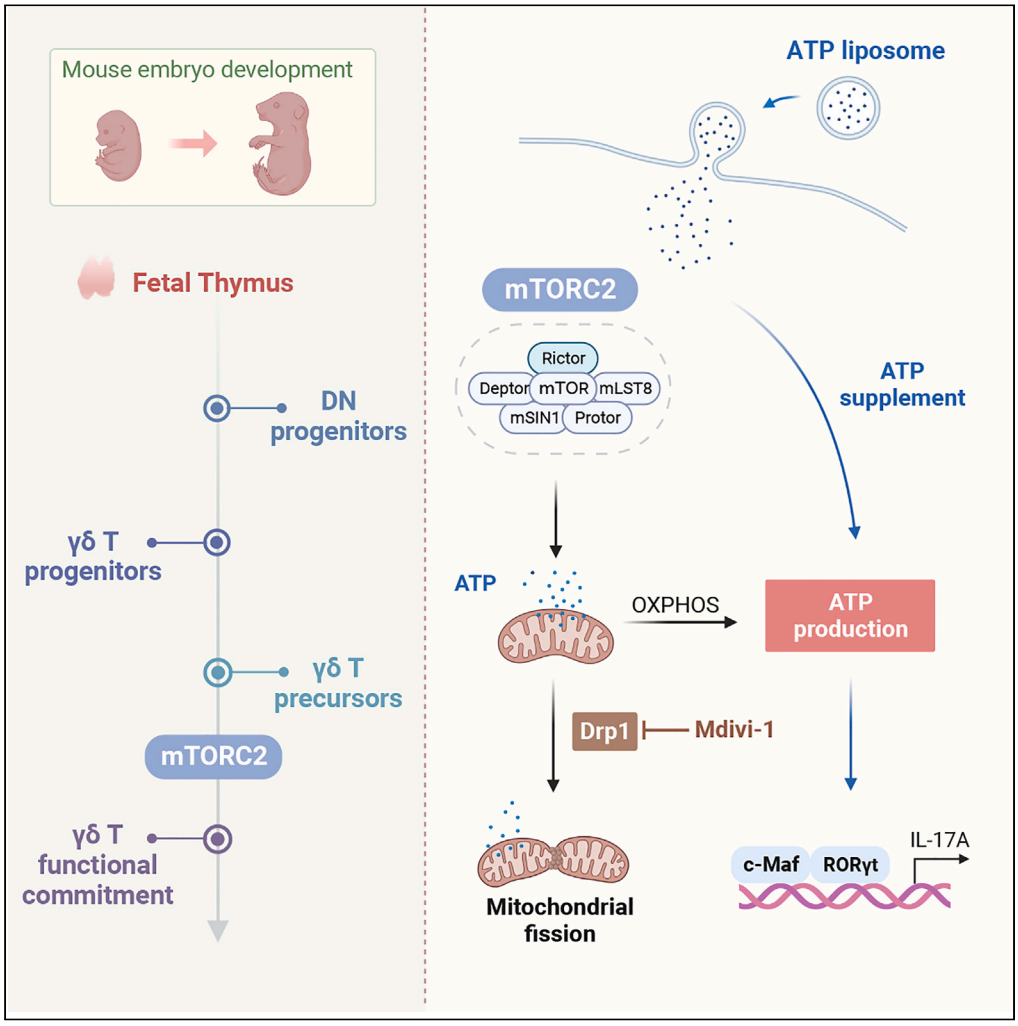

Yunke Wang, Hui Qin, Yihua Cai, ..., Jie Zheng, Fuming Qiu, Jun Yan

jun.yan@louisville.edu

Highlights

mTORC2 controls thymic commitment of γδT17 cells via transcription factor c-Maf

mTORC2 deficiency results in impaired mitochondrial fission and ATP production

Drp1 is a key metabolic checkpoint of γδT17 cells

ATP reconstitution rescues thymic γδT17 defect caused by mTORC2 deficiency

Wang et al., iScience 26, 106630
May 19, 2023
https://doi.org/10.1016/j.isci.2023.106630

iScience

CellPress
OPEN ACCESS

Article

Natural γδT17 cell development and functional acquisition is governed by the mTORC2-c-Maf-controlled mitochondrial fission pathway

Yunke Wang,[1,2,3,11] Hui Qin,[1,4,11] Yihua Cai,[1] Xu Chen,[1,5] Hong Li,[6] Diego Elias Montoya-Durango,[1] Chuanlin Ding,[1] Xiaoling Hu,[1] Julia H. Chariker,[7,8] Harshini Sarojini,[1] Sufan Chien,[1] Eric C. Rouchka,[8,9] Huang-Ge Zhang,[10] Jie Zheng,[4] Fuming Qiu,[2,3] and Jun Yan[1,12,*]

SUMMARY

Natural IL-17-producing γδ T cells (γδT17 cells) are unconventional innate-like T cells that undergo functional programming in the fetal thymus. However, the intrinsic metabolic mechanisms of γδT17 cell development remain undefined. Here, we demonstrate that mTORC2, not mTORC1, selectively controls the functional fate commitment of γδT17 cells through regulating transcription factor c-Maf expression. scRNA-seq data suggest that fetal and adult γδT17 cells predominately utilize mitochondrial metabolism. mTORC2 deficiency results in impaired Drp1-mediated mitochondrial fission and mitochondrial dysfunction characterized by mitochondrial membrane potential ($\Delta\Psi m$) loss, reduced oxidative phosphorylation (OXPHOS), and subsequent ATP depletion. Treatment with the Drp1 inhibitor Mdivi-1 alleviates imiquimod-induced skin inflammation. Reconstitution of intracellular ATP levels by ATP-encapsulated liposome completely rescues γδT17 defect caused by mTORC2 deficiency, revealing the fundamental role of metabolite ATP in γδT17 development. These results provide an in-depth insight into the intrinsic link between the mitochondrial OXPHOS pathway and γδT17 thymic programming and functional acquisition.

INTRODUCTION

Unconventional innate-like γδ T cells are mainly subdivided into IFN-γ-producing γδ T (γδT1) and IL-17-producing γδ T (γδT17) subsets. Most of them acquire functional capacity in the fetal thymus[1]. The emergence of murine thymic γδ T cells is often described as successive and coordinated waves characterized by distinct Vγ usages.[2,3] γδT17 cells composed of Vγ4, Vγ6, and a few Vγ1 (Heilig and Tonegawa nomenclature)[4] are reported to emerge around embryonic 16.5 days (E16.5). They are the main producer of IL-17A which underpins its plasticity in response to innate stimuli in different disease settings such as cancer, autoinflammatory diseases, and infectious diseases. γδT17 cells drive tumor progression and metastasis by promoting angiogenesis and interacting with myeloid-derived suppressor cells and neutrophils to form an immunosuppressive tumor microenvironment.[5–7] γδT17 cells are also critical in maintaining autoimmune-related tissue homeostasis and infection surveillance.[8,9] Understanding the molecular basis of γδT17 functional acquisition helps further investigate IL-17A-related immunopathogenesis.

The mechanism controlling the thymic commitment of γδT17 is not fully understood. T cell antigen receptor (TCR) signaling strength is a widely accepted factor that determines the functional fate of thymic γδ T cells. Accumulating evidence suggests that strong TCR signaling promotes γδT1 development while prohibits γδT17 commitment.[10–12] However, reduced TCR signaling shown in CD3 double haploinsufficient mice[13] or ZAP70-deficient SKG mice[14] drastically impairs γδT17 commitment, suggesting that TCR signaling may be still prerequisite for IL-17 producers. There are a number of other factors involved in γδT17 commitment. The high-mobility group (HMG) transcriptional factor SOX4 and SOX13 and their upstream factor HEB are essentially required for γδT17 generation by directly regulating γδT17 cell-specific gene *Rorc*.[15–17] Transcription factor c-Maf has been identified as a universal regulator of γδT17 differentiation and its expression is altered by γδTCR signal strength.[18] SOX13/c-Maf/RORγt program sequentially supports γδT17 ontogeny.[19] The zinc-finger transcription factor PLZF governs the development of Vγ6

[1]Division of Immunotherapy, The Hiram C. Polk, Jr., MD Department of Surgery, Immuno-Oncology Program, Brown Cancer Center, University of Louisville, Louisville, KY, USA

[2]Key Laboratory of Tumor Microenvironment and Immune Therapy of Zhejiang Province, The Second Affiliated Hospital, Zhejiang University School of Medicine, Hangzhou, Zhejiang, China

[3]Department of Medical Oncology, The Second Affiliated Hospital, Zhejiang University School of Medicine, Hangzhou, Zhejiang, China

[4]Department of Dermatology, Shanghai Jiaotong University Ruijin Hospital, Shanghai, China

[5]Department of Clinical Immunology, Shanghai Ninth People's Hospital, Shanghai Jiao Tong University School of Medicine, Shanghai, China

[6]Functional Immunomics Core, Brown Cancer Center, University of Louisville, Louisville, KY, USA

[7]Department of Anatomical Sciences and Neurobiology, University of Louisville, Louisville, KY, USA

[8]Kentucky Biomedical Research Infrastructure Network Bioinformatics Core University of Louisville, Louisville, KY, USA

[9]Department of Biochemistry and Molecular Genetics, University of Louisville, Louisville, KY, USA

[10]Department of Microbiology and Immunology, Brown Cancer Center, University of Louisville, Louisville, KY, USA

Continued

γδT17 cells,[20] while the HMG transcription factor TCF1 abrogates γδT17 cell generation through E protein.[15,21] Transforming growth factor-β1 (TGF-β1),[22] Notch/Hes1 signaling,[23] SLAM/SAP signaling,[24] and Syk/phosphoinositide 3-kinase (PI3K)/Akt signaling[25] have also been reported to facilitate γδT17 development. The deficiency of ubiquitin-like containing plant homeodomain (PHD) ring finger 1 (UHRF1) enhances γδT17 differentiation by epigenetic regulation of early growth response 1 (EGR1).[26]

Metabolic programming also controls the functional fate of γδ T cells. A recent study reports that γδT1 cells favor glycolysis, while γδT17 cells strongly rely on oxidative metabolism with higher mitochondrial mass and activity.[27] Reduced efficiency of glycolysis or oxidative phosphorylation (OXPHOS) pathway in fetal thymic organ cultures (FTOC) directly promotes or impairs γδT17 development. Combined with our previous findings that γδT17 cells predominately adopt the OXPHOS pathway for energy fuel,[28] we then raise the question of how mitochondrial OXPHOS activity impacts γδT17 early development and functional programming.

The mechanistic or mammalian target of the rapamycin (mTOR) signaling pathway plays a central role in cell proliferation, metabolism, and differentiation.[29–31] mTOR is composed of two complexes, mTOR complex 1 (mTORC1) and 2 (mTORC2), which are characterized by distinct scaffolding proteins, Raptor (regulatory associated protein of mTOR) and Rictor (rapamycin-insensitive companion of mTOR), respectively. We[28] and others[32] showed that mTORC1 was involved in the proliferation of γδ T cells, and mTORC2 deficiency strongly impacted γδT17 effector function by dysfunctional mitochondria accumulation and mitochondrial reactive oxygen species (ROS) production. However, it is unknown whether mTOR signaling is involved in the thymic functional commitment of γδT17 cells.

Here, we aim to determine the intrinsic link between γδT17 thymic programming and mitochondrial OXPHOS pathway. We demonstrate that mTORC2 selectively regulates the thymic commitment of γδT17 cells through c-Maf expression. mTORC2 deficiency results in impaired Drp1-mediated mitochondrial fission and mitochondrial dysfunction characterized by mitochondrial membrane potential ($\Delta\Psi m$) loss and subsequent ATP depletion. Reconstitution of ATP completely rescues thymic γδT17 defect caused by mTORC2 deficiency. These findings suggest that γδT17 thymic commitment is governed by the mTORC2-mediated metabolic reprogramming.

RESULTS

mTORC2 controls γδT17 development during ontogeny in the thymus

To determine the role of mTORC1 and mTORC2 in γδT17 during thymic development, we used $CD2^{cre}$ $Raptor^{fl/fl}$ (Raptor conditional knockout (cKO)) and $CD2^{cre}$ $Rictor^{fl/fl}$ (Rictor cKO) mice,[28] and chose E18/E20/new-born Day1 (D1) as the experimental time points according to the occurrence of γδT17 in the late perinatal period. Flow gating strategy was shown in Figure S1. Compared to its control littermates, E18, E20, and D1 Raptor cKO thymocytes showed no difference in the percentages of total γδ T and two main γδT17 subsets, Vγ4 and Vγ6 (Figures S2A–S2D, S3A, and S3B). E18, E20, and D1 Rictor cKO mice showed a slight reduction in the absolute number and the percentage of Vγ6 cells (Figures S3C, S3D, and S4A), whereas no significant alteration was found in total γδ T and Vγ4 cells (Figures 1A, S3C, and S3D). The transcription factor RORγt and the tumor necrosis factor receptor family CD27 are previously identified to segregate γδT17 and γδT1.[33] We then examined $CD27^{-}$, $ROR\gamma t^{+}$, and $CD27^{-}ROR\gamma t^{+}$ populations as well as intracellular cytokine IL-17/IFN-γ expression in total γδ T, Vγ4, and Vγ6 cells. Raptor cKO thymocytes on E18, E20, and D1 showed no difference in $CD27^{-}$, $ROR\gamma t^{+}$, $CD27^{-}ROR\gamma t^{+}$ γδ T cells, and IL-17/IFN-γ expression (Figures S2B, S3A, and S3B). In contrast, Rictor cKO thymocytes on E18, E20, and D1 demonstrated reduced percentages and absolute numbers of $ROR\gamma t^{+}$ γδ T cells and IL-17 production. However, IFN-γ production was not altered (Figures 1B, S3C, S3D, and S4A). Similar results were found in both Vγ4 and Vγ6 subsets (Figures 1C, 1D, S2C, S2D, S3A-S3D, and S4A), suggesting that mTORC2, but not mTORC1, regulates functional commitment of γδT17 cells during embryonic development in the thymus.

mTORC2 deficiency selectively impacts on the functional acquisition of γδT17 cells from γδ T precursors

γδ T cells are reported to acquire the ability to produce IL-17 at E16.5.[2] To determine how early mTORC2 signaling influences the functional acquisition of γδT17 cells, we analyzed IL-17 and IFN-γ production in γδ T cells from E16/E17/E18/E19 Rictor cKO fetal thymus. We observed the reduced IL-17 production from γδ

[11]These authors contributed equally

[12]Lead contact

*Correspondence: jun.yan@louisville.edu

https://doi.org/10.1016/j.isci.2023.106630

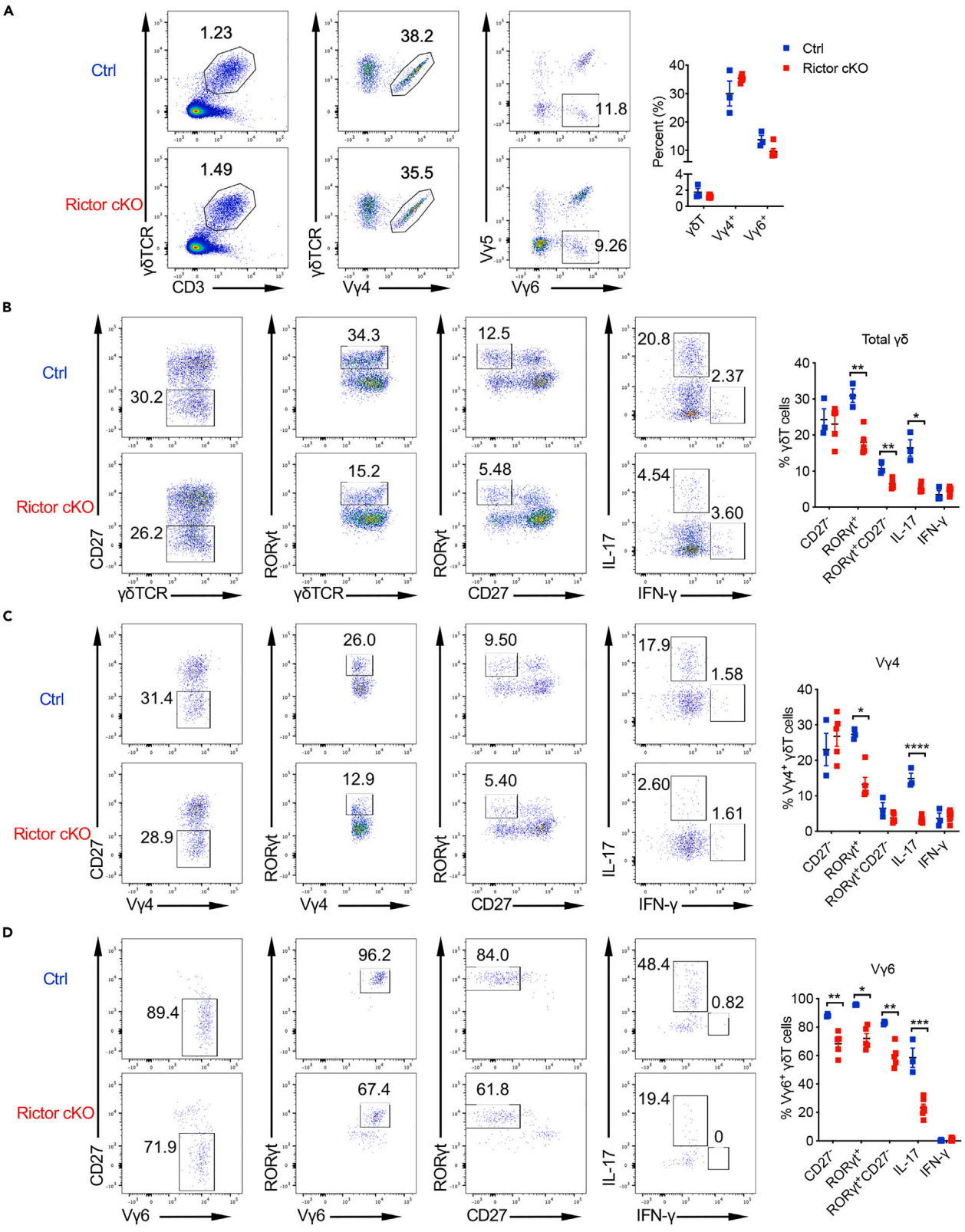
A
Ctrl
Rictor cKO
1.23
1.49
38.2
35.5
11.8
9.26
γδTCR
CD3
Vγ4
Vγ5
Vγ6
Percent (%)
γδT
Vγ4+
Vγ6+
Ctrl
Rictor cKO
B
30.2
26.2
34.3
15.2
12.5
5.48
20.8
2.37
4.54
3.60
CD27
RORγt
IL-17
IFN-γ
Total γδ
% γδT cells
CD27-
RORγt+
RORγt+CD27-
C
31.4
28.9
26.0
12.9
9.50
5.40
17.9
1.58
2.60
1.61
Vγ4
% Vγ4+ γδT cells
D
89.4
71.9
96.2
67.4
84.0
61.8
48.4
0.82
19.4
0
Vγ6
% Vγ6+ γδT cells

Figure 1. mTORC2 alters γδT17 development in fetal thymus

Cells from Embryonic 18 days (E18) Rictor$^{fl/fl}$ and CD2^{cre} Rictor$^{fl/fl}$ fetal thymus were stimulated with phorbol myristate acetate (PMA)/I for 5 h and analyzed by flow cytometry (n = 3–5/each group).

(A) Flow plots of γδ T were gated on live cells. Vγ4$^+$γδ T and Vγ5$^-$Vγ6$^+$γδ T cells (Mann-Whitney test) were gated on live CD3$^+$γδTCR$^+$ cells. Representative dot plots and summarized data are shown.

(B) Flow plots of CD27$^-$γδ T, RORγt$^+$γδ T, RORγt$^+$CD27$^-$γδ T cells and intracellular IL-17/IFN-γ production were gated on CD3$^+$γδTCR$^+$ cells. Representative dot plots and summarized data are shown.

(C) Flow plots of CD27$^-$Vγ4$^+$γδ T, RORγt$^+$Vγ4$^+$γδ T, RORγt$^+$CD27$^-$Vγ4$^+$γδ T cells, and intracellular IL-17/IFN-γ production were gated on CD3$^+$γδTCR$^+$Vγ4$^+$ cells.

(D) Flow plots of CD27$^-$Vγ6$^+$γδ T, RORγt$^+$Vγ6$^+$γδ T (Mann-Whitney test), RORγt$^+$CD27$^-$Vγ6$^+$γδ T cells, and intracellular IL-17/IFN-γ production were gated on CD3$^+$γδTCR$^+$Vγ5$^-$Vγ6$^+$ cells. Representative dot plots and summarized data are shown. Data are representative of at least three independent experiments with similar results. Data are shown as mean ± SEM. Unpaired Student's *t* test (A-D) and Mann-Whitney test (A, C) were used. *p < 0.05, **p < 0.01, ***p < 0.001, ****p < 0.0001.

T cells in E16-E19 Rictor cKO mice (Figure 2A), suggesting that mTORC2 regulates γδT17 differentiation before they acquire effector function. We next examined whether mTORC2 has a role in the early development of T cell progenitors. T cell progenitors sequentially undergo double-negative (DN, CD4$^-$CD8$^-$), double-positive (DP, CD4$^+$CD8$^+$), and single-positive (SP, CD4$^+$CD8$^-$ or CD4$^-$CD8$^+$) stages after being seeded in the thymus. Thymocytes of E18 Rictor cKO mice showed increased percentages of DN and CD8 SP cells, and decreased percentage and absolute number of DP cells (Figures 2B and S4B), suggesting that mTORC2 deficiency might impair DN-DP transition in T cell development. Functional γδTCR expression drives DN2 (CD44$^+$CD25$^+$) or DN3 (CD44$^-$CD25$^+$) cells into γδ T cell lineage.[34] We thus examined DN thymocytes by CD25 and CD44 expression. We found no difference in the proportions and absolute numbers of DN1 (CD44$^+$CD25$^-$), DN2, DN3, and DN4 (CD44$^-$CD25$^-$) (Figures 2C and S4B). TCR signaling-dependent CD73 expression marks the commitment of γδ T cell precursors into γδ T cell lineage. We observed no significant difference in the percentages and absolute numbers of uncommitted (CD24$^+$CD73$^-$; uncom.) and committed γδ T cells (CD24$^+$CD73$^+$; Com.), while reduced absolute numbers of mature (CD24$^-$CD73$^+$) γδ T cells (Figures 2D and S4B). Given the fact that there was no difference in the percentage and absolute number of total γδ T cells from Rictor cKO fetal thymus (Figure 1A), we hypothesized that mTORC2 may not be indispensably involved in the commitment of γδ T cell progenitors to γδ T lineage. CD27$^-$CD44$^+$ γδ T cells are exclusively segregated to γδT17 lineage.[10,27] Rictor deficient fetal thymus showed decreased CD24$^-$CD27$^-$CD44$^+$ mature γδ T cells and CD24$^+$RORγt$^+$ immature Vγ4 T cells (Figures 2D, 2E, and S4B). c-Maf was firstly detected in CD25$^+$CD27$^+$ precursors and induced RORγt expression in later CD25$^-$CD27$^+$ period.[18] Rictor deficiency resulted in accumulated CD25$^+$CD27$^+$ precursors (Figure 2G), indicating that loss of Rictor hinders the process where γδ T cells should sequentially acquire IL-17-related profiles during development. Collectively, these data reveal that mTORC2 deficiency selectively impairs the functional acquisition of γδT17 cells in the thymus.

mTORC2 regulates γδT17 commitment and effector function through c-Maf expression

Given the critical role of c-Maf in γδT17 cell commitment,[18] we evaluated the expression of c-Maf within the γδT17 compartment in E18 Rictor cKO fetal thymus. mTORC2 deficiency led to a drastic reduction of c-Maf expression in total γδ T, Vγ4, and Vγ6 γδ T cells (Figure 3A). We further examined IL-17 and IFN-γ production of γδ T cells from E18, E20, and D1 Rorc^{cre} c-Maf$^{fl/fl}$ fetal thymi. We confirmed that IL-17 production was significantly decreased in total γδ T, Vγ4, and Vγ6 γδ T cells (Figures 3B, S5A, and S5B), consistent with previous reports.[18] To determine the direct role of c-Maf in mTORC2-dependent γδT17 effector function, we pre-activated purified γδ T cells from pooled Rictor cKO mice and transduced them with c-Maf and control lentivirus. c-Maf lentivirus infection upregulated c-Maf expression in Rictor cKO γδ T cells (Figure 3C). Consequently, IL-17 production was significantly increased in c-Maf lentivirus-infected γδ T cells from Rictor cKO mice while IFN-γ production remained unchanged (Figure 3D). Together, these data indicate that mTORC2 deficiency impacts γδT17 commitment and effector function through down-regulating c-Maf expression.

γδT17 cells exhibit dominate mitochondrial metabolism

To explore possible mechanisms underlying the impact of mTORC2 on γδT17 commitment and effector function, single-cell RNA sequencing (scRNA-seq) was used to profile γδ T cells. Pan γδ T cells were sorted from the spleen and lymph nodes (LNs) of naive mice. After removing low-quality cells based on low total transcript numbers, total of 7,675 cells from two independent experiments (3,888 and 3,687 cells, respectively) were subjected to analysis. Total 17 clusters were characterized based on the maker genes, showing γδ T cell heterogeneity in the periphery (Figure 4A). Three clusters (clusters 10, 11, and 12) highly expressed

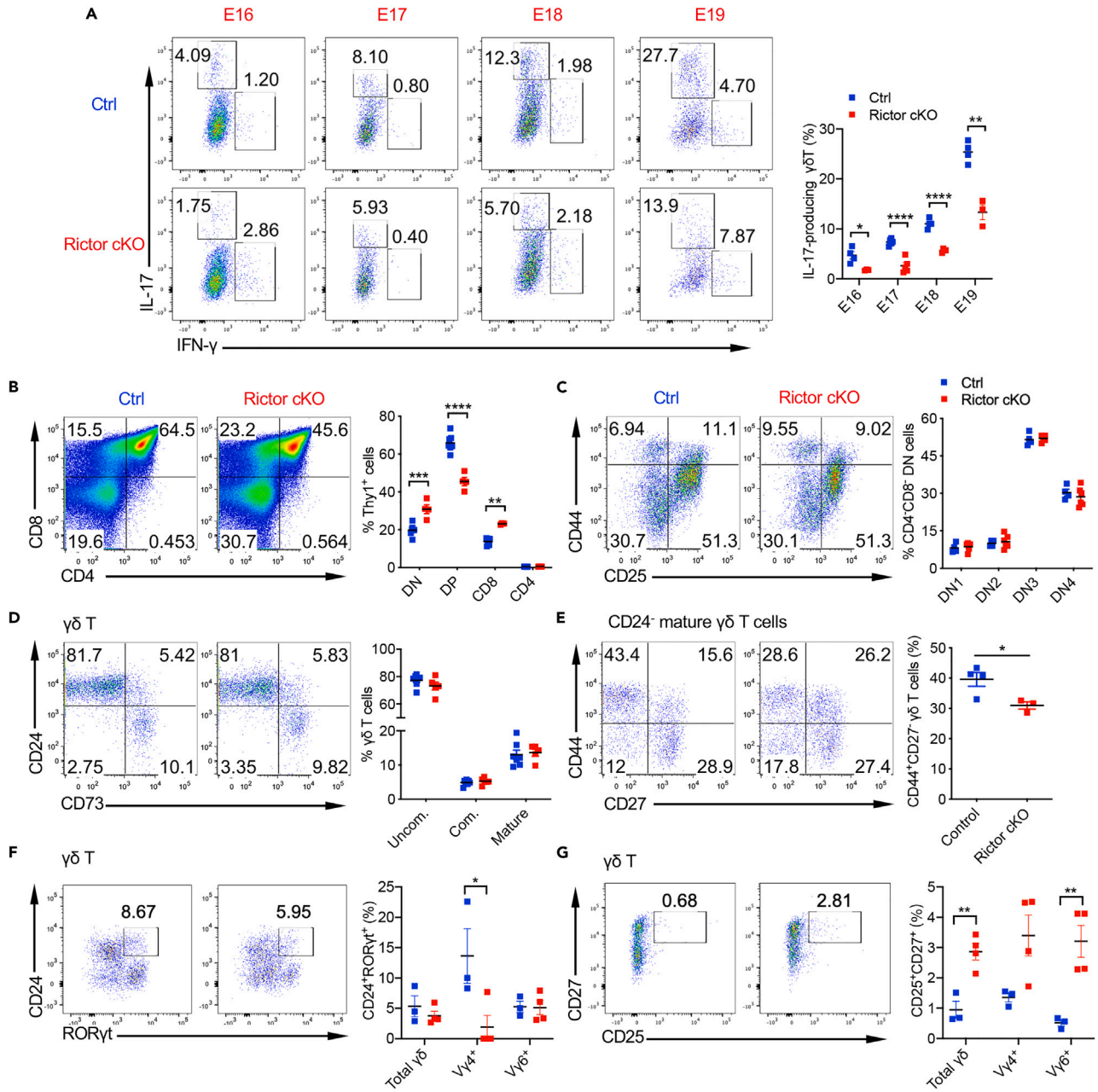

Figure 2. mTORC2 selectively impacts on the functional pre-programming stage of γδT17 cells

(A) Cells from E16/E17/E18/E19 Rictor$^{fl/fl}$ and CD2^{cre} Rictor$^{fl/fl}$ fetal thymus were stimulated with PMA/I for 5h and intracellular IL-17/IFN-γ production by γδ T cells were assessed by flow cytometry (n = 3–6/each group).

(B–G) Cells from E18 Rictor$^{fl/fl}$ and CD2^{cre} Rictor$^{fl/fl}$ fetal thymus were analyzed for surface expression of Thy1, CD3, CD4, CD8, TCRγδ, CD44, CD25, CD24, CD73, CD27, RORγt, and CD25 (n = 3–7/each group). (B) Flow plots of CD4 (CD4$^+$CD8$^-$), CD8 (CD4$^-$CD8$^+$) (Mann-Whitney test), DP (CD4$^+$CD8$^+$), and DN (CD4$^-$CD8$^-$) cells were pre-gated on Thy1$^+$ cells. (C) Flow plots of DN1 (CD44$^+$CD25$^-$), DN2 (CD44$^+$CD25$^+$), DN3 (CD44$^-$CD25$^+$), and DN4 (CD44$^-$CD25$^-$) were pre-gated on Thy1$^+$CD4$^-$CD8$^-$ DN cells. (D) Flow plots of uncommitted (Uncom.; CD24$^+$CD73$^-$), committed (Com.; CD24$^+$CD73$^+$), and mature (CD24$^-$CD73$^+$) γδ T cells were pre-gated on Thy1$^+$CD4$^-$CD8$^-$TCRγδ$^+$ cells. (E) Flow plots of CD44$^+$CD27$^-$ γδ T cells were gated on Thy1$^+$CD4$^-$CD8$^-$TCRγδ$^+$CD24$^-$ mature γδ T cells. Flow plots of CD24$^+$RORγt$^+$ (F) and CD25$^+$CD27$^+$ (G) cells were gated on CD3$^+$TCRγδ$^+$ cells. Summarized data show their percentages in total γδ T, Vγ4 and Vγ6 cells, respectively. Data are representative of at least two independent experiments with similar results. Summarized data are shown as mean ± SEM. Unpaired Student's *t* test (A-G) and Mann-Whitney test (B) were used. *p < 0.05, **p < 0.01, ***p < 0.001, ****p < 0.0001.

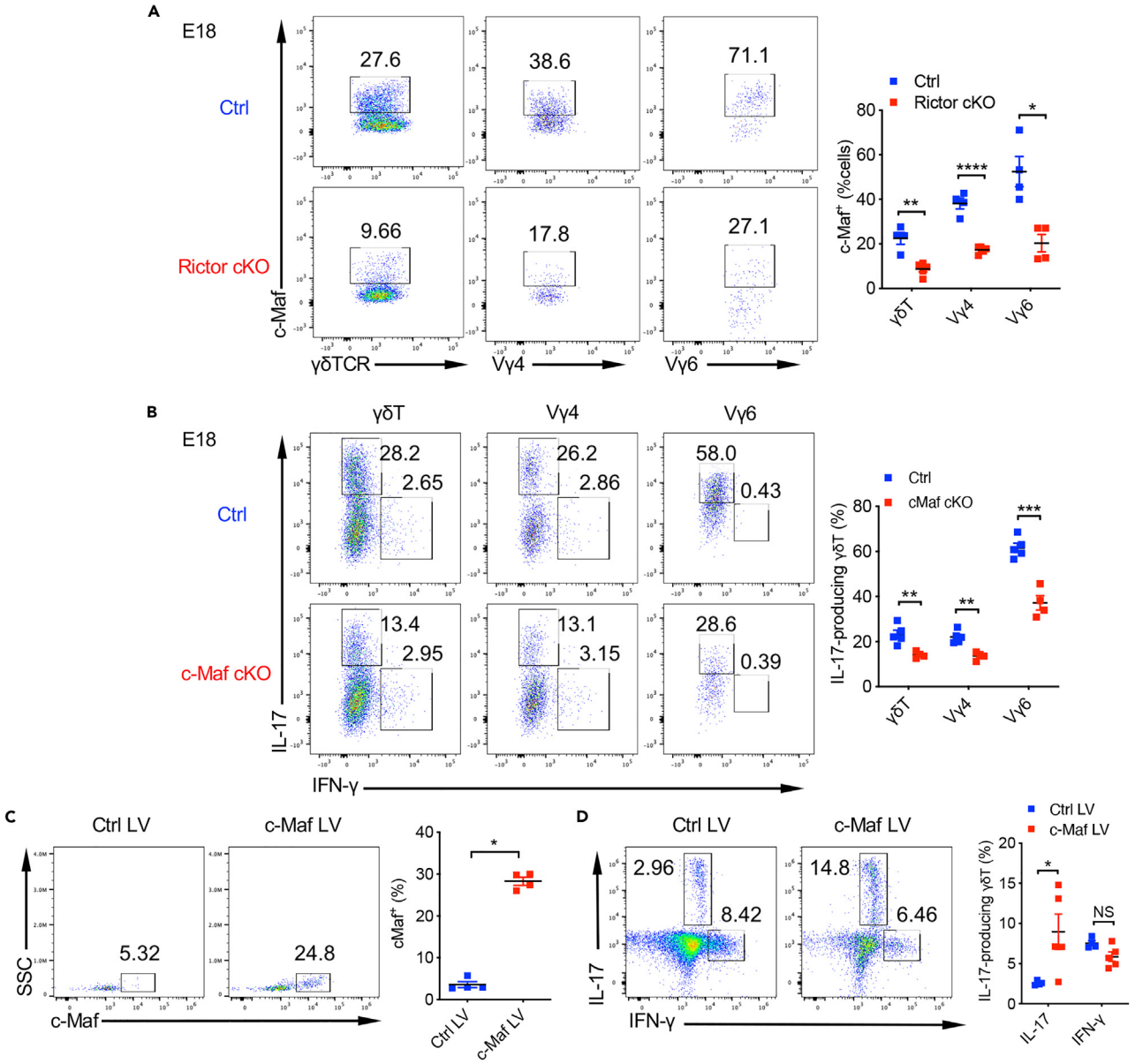

Figure 3. mTORC2 deficiency impairs c-Maf expression with decreased γδT17 cells

(A) c-Maf expression in thymocytes of E18 Rictor$^{fl/fl}$ and CD2^{cre} Rictor$^{fl/fl}$ mice were analyzed by flow cytometry (n = 4/each group). Flow plots were gated on CD3$^+$TCRγδ$^+$, CD3$^+$TCRγδ$^+$Vγ4$^+$, or CD3$^+$TCRγδ$^+$Vγ6$^+$ (Mann-Whitney test) cells. Representative dot plots and summarized data are shown.

(B) Cells from E18 c-Maf$^{fl/fl}$ and Rorc^{cre} c-Maf$^{fl/fl}$ fetal thymus were stimulated with PMA/I for 5 h and intracellular IL-17/IFN-γ production by γδ T cells and different subsets (Vγ4 and Vγ6) were assessed by flow cytometry (n = 4–5/each group). Representative dot plots and summarized data are shown.

(C and D) *in vitro* cultured γδ T cells from peripheral LNs of CD2^{cre} Rictor$^{fl/fl}$ mice were transduced with control or c-Maf lentivirus at a final concentration of 10 m.o.i (n = 4–5/each group). Cells were cultured with rmIL-23 (10 ng/ml) plus rmIL-1β (10 ng/ml) for another 2 days, and incubated with Golgi-Plug at 37°C for 4 h. c-Maf expression (C) and IL-17/IFN-γ production (D) by γδ T cells were analyzed by flow cytometry. Data are representative of at least two independent experiments with similar results. Data are shown as mean ± SEM. Unpaired Student's *t* test (A, B, D) and Mann-Whitney test (B, C) were used. *p < 0.05, **p < 0.01, ***p < 0.001, ****p < 0.0001; NS, not significant.

Maf (Figure 4B). Clusters 10 and 12 also expressed high levels of *Il17a* and *Rorc*, suggesting γδT17 clusters. Since c-Maf is firstly expressed in γδ T precursors and subsequently induces downstream RORγt expression which jointly prompts precursors to acquire IL-17-related profiles,[18] cluster 11 was considered as a transitional status of γδ T cells which acquires IL-17 phenotype later. Interestingly, *Rictor* gene expression was high in all clusters while *Rptor* gene expression levels were low (Figure 4B). Clusters 0, 6, and 9 highly

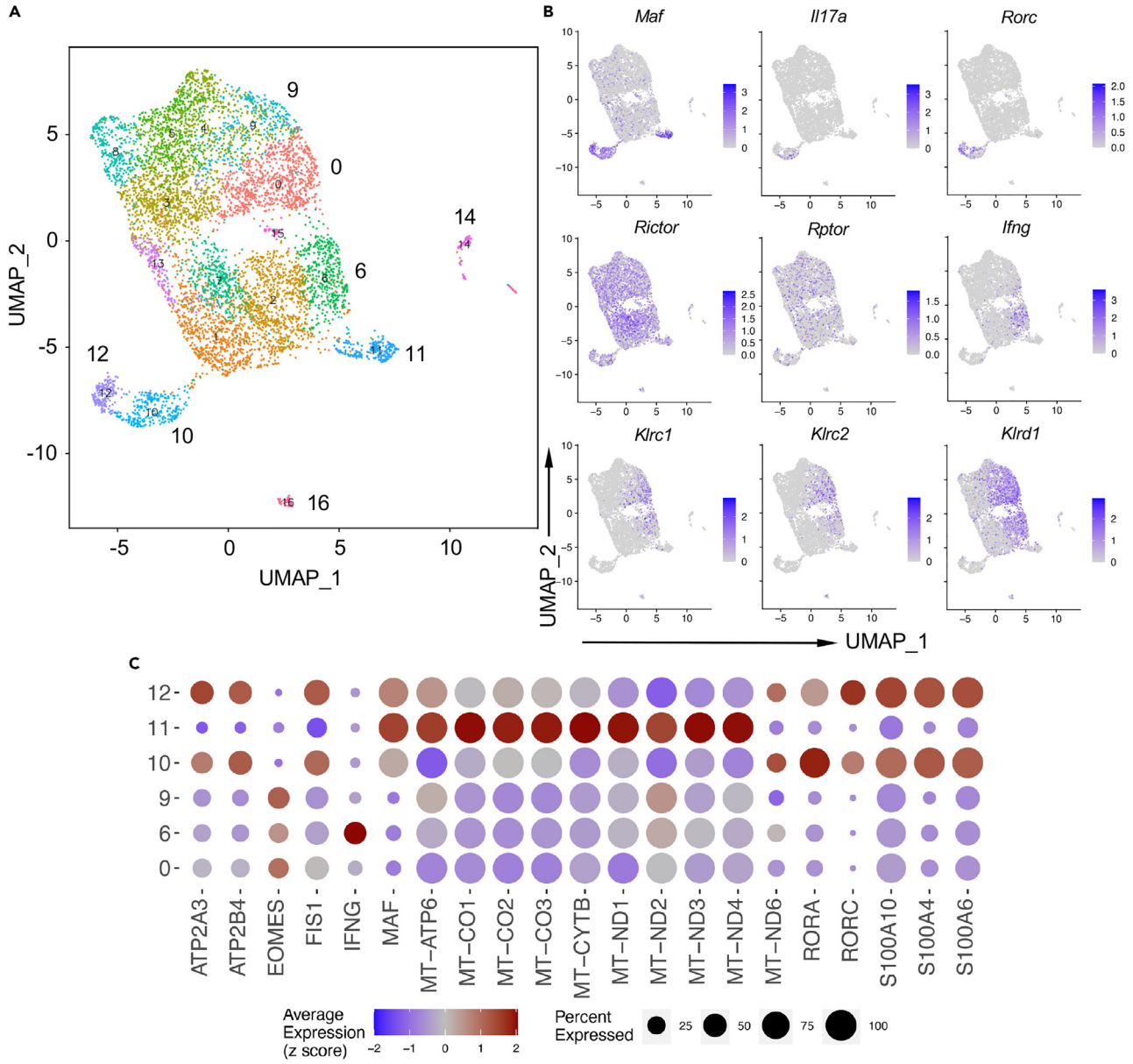

Figure 4. γδT17 clusters highly express mitochondrial functionally related genes

Pan γδ T cells were sorted from spleen and LNs of naive mice for scRNA-seq.

(A) Uniform manifold approximation and projection (UMAP) analysis displayed 17 color-coded cell clusters in the combined scRNA-seq datasets of pan γδ T. n = 7675 cells.

(B) Feature plots showing expression levels of *Maf*, *Il17a*, *Rorc*, *Rictor*, *Rptor*, *Ifng*, *Klrc1*, *Klrc2*, and *Klrd1* across all clusters.

(C) Dot plots displayed average scaled expression levels (z-scores) of indicated genes in clusters 0, 6, 9, 10, 11, and 12. Dot size reflects the percentage of cells expressing the selected gene in each cell cluster.

expressed *Ifng*, *Klrc1*, *Klrc2*, and *Klrd1*, suggesting γδT1 clusters. Dot plot analysis further confirmed that clusters 10, 11, and 12 highly expressed *Maf*, *Rora*, and *Rorc* while clusters 0, 6, and 9 highly expressed *Eomes* and *Ifng*. We also found that c-Maf expressing clusters highly expressed ATPase-related genes, mitochondrially encoded cytochrome *c*/B oxidase genes (respiratory complex IV), mitochondrially encoded nicotinamide adenine dinucleotide + hydrogen (NADH) dehydrogenase genes (respiratory complex I), and mitochondrially encoded ATP synthase (respiratory complex V) gene *mt-Atp6* (Figure 4C). Mitochondrial fission gene *Fis1* was also highly expressed on clusters 10 and 12. To further strengthen our conclusion, we used publicly available datasets in which scRNA-seq was performed to determine the regulatory

landscape of fetal and adult γδ T cell development.[19] These scRNA-seq data generated from fetal thymus were analyzed and total of 12 γδ T cell clusters were identified (Figure S6A). Notably, cluster 4 expressed high levels of *Maf*, *Rorc*, *Sox13*, and *Blk*, representing the γδT17 cluster. While cluster 5 expressed high levels of *Klrc2* and *Klrd1* representing cytotoxic γδ T cells (Figure S6B). Dot plot data showed that cluster 4 also expressed high levels of mitochondrial function-related genes including *Atp13a3*, *Atp6v0d1*, *Atp6v1g1*, and *Atp8b4* compared to cluster 5 (Figure S6C). Taken together, these data collectively suggest the dominant mitochondrial metabolism in fetal and adult γδT17 cells.

mTORC2 deficiency inhibits Drp1-mediated mitochondrial fission in γδT17 cells

As a highly dynamic ultrastructure, mitochondria need to keep a balance between mitochondrial fission and fusion.[35] Any perturbations of mitochondrial dynamics could result in mitochondrial dysfunction. We hypothesized that the mitochondrial dysfunction caused by mTORC2 deficiency might be due to the defect of mitochondrial fission which is governed by dynamin-related protein 1 (Drp1). Drp1 is the key pro-fission protein that is recruited from the cytosol to mitochondrial membranes where it oligomerizes and forms a ring-like structure to execute membrane constriction. Prior evidence has shown that mTORC1 promotes mitochondrial fission by 4E (eIF4E)-binding proteins (4E-BPs)/mitochondrial fission process 1 (MTFP1)/Drp1 axis in mouse embryonic fibroblasts.[36] However, whether mTORC2 links with mitochondrial fission in γδ T cells remains unknown.

We observed decreased $\Delta\Psi m$ in CD27$^-$ γδ T cells from Rictor cKO fetal thymus, as defined by tetramethylrhodamine methyl ester (TMRM) staining (Figure 5A). The phosphorylation of Drp1 (*p*-Drp1) in γδ T cells was upregulated by IL-1β and IL-23 stimulation. *p*-Drp1 levels in CD27$^-$ γδ T cells were significantly increased in control mice while no increase was noted in these from Rictor cKO E18 fetal thymus (Figure 5B) or adult peripheral LNs (Figure 5C), suggesting that mTORC2 deficiency may lead to decreased Drp1-mediated mitochondrial fission in γδT17 cells. To determine whether intervening Drp1 signaling could affect the function of γδT17 cells, we treated γδ T cells from adult wildtype (WT) mice with Drp1 inhibitor Mdivi-1, which induced less than 15% cell death, and found IL-17 production was significantly reduced in a dose-dependent manner (Figure 5D). Likewise, *in vivo* Mdivi-1 treatment decreased IL-17 production while IFN-γ production was not altered from γδ T cells (Figure 5E). In addition, transcription factor RORγt and c-Maf expression levels were also significantly reduced (Figure 5F). Collectively, these results suggest that the altered γδT17 development and effector function caused by mTORC2 ablation is likely due to defective mitochondrial fission pathway.

IMQ-induced skin inflammation is ameliorated in Mdivi-1-treated mice

Having demonstrated the critical role of mitochondrial fission pathway in regulating γδT17 cell commitment and effector function, we examined whether inhibition of mitochondrial fission can ameliorate imiquimod (IMQ)-induced skin inflammation. Previous studies have shown that dermal γδT17 cells play a critical role in IMQ-induced psoriasis-like mouse model.[8,37] To this end, mice applied with topical IMQ were also treated with Drp-1 inhibitor Mdivi-1 or vehicle control (Figure 6A). Gross skin images showed less severe inflammation in Mdivi-1-treated mice compared to these in vehicle control-treated mice (Figure 6B). Histological analysis showed that Mdivi-1-treated mice had significantly decreased epidermal thickness compared to vehicle-treated mice (Figure 6C). Flow cytometry analysis indicated that neutrophil infiltration (Figure 6D) and spontaneous IL-17 production of dermal γδ T cells from Mdivi-1-treated mice was significantly reduced as compared with vehicle control-treated mice (Figure 6E), whereas this phenotype was not observed in naive mice without IMQ application (Figure S7). Similarly, IL-17 production of γδ T cells upon stimulation was also reduced in skin draining LNs (Figure 6E). We also used imaging mass cytometry (IMC) to analyze skin tissues and found that mouse skin from Mdivi-1-treated mice displayed much less infiltrations of CD11b$^+$ myeloid cells and F4/80$^+$ macrophages (Figure 6F). uMAP analysis showed that F4/80^{hi} and F4/80^{low} macrophages and neutrophils were substantially reduced in the skin from Mdivi-1-treated mice (Figure 6G). These results illustrate that inhibition of mitochondrial fission helps alleviate IMQ-induced skin inflammation possibly through reduced dermal γδT17 cells.

Cellular ATP level governs the function of γδT17 cells in metabolically impaired or intact state

Mitochondrial dysfunction is characterized by $\Delta\Psi m$ loss, inefficient OXPHOS, and ATP depletion.[38,39] We[28,40] and others[27] previously reported that γδT17 cells predominately use OXPHOS pathway, which is the main source of ATP production. Indeed, a sharp reduction in ATP level was observed in γδ T cells from E18 Rictor cKO thymus compared to its control littermates (Figure 7A). To further investigate whether reduced ATP production caused by mTORC2 deficiency directly accounts for defective γδT17 effector

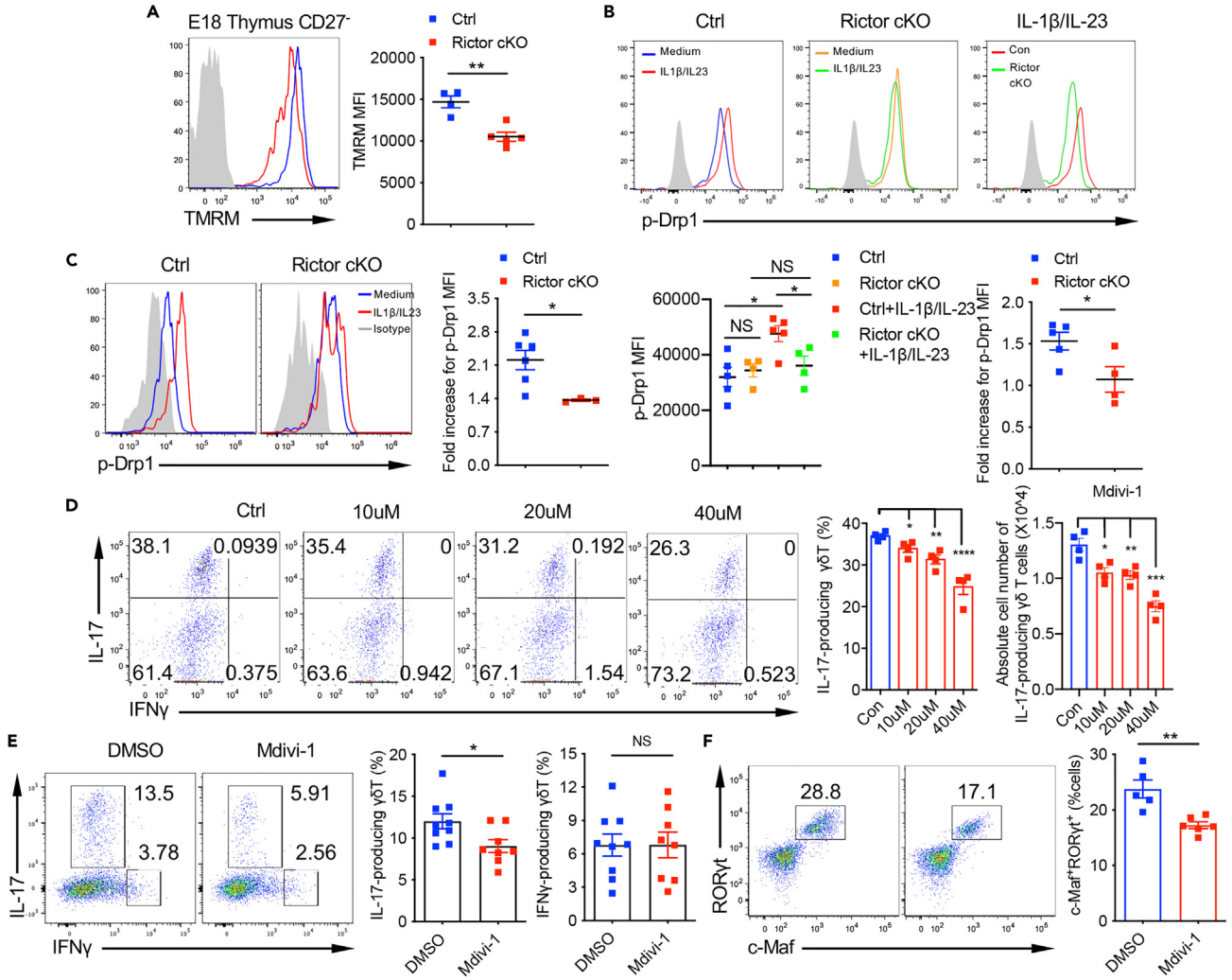

Figure 5. mTORC2 deficiency abrogates γδT17 functional acquisition and effector function by inhibiting Drp1-mediated mitochondrial fission

(A) Thymocytes from E18 Rictor$^{fl/fl}$ and CD2^{cre} Rictor$^{fl/fl}$ mice were stained with TMRM for mitochondrial membrane potential (n = 4–5/each group). Flow histograms were gated on CD3$^+$TCRγδ$^+$CD27$^-$ cells. Representative dot plots and summarized data are shown.

(B and C) Thymocytes from E18 Rictor$^{fl/fl}$ and CD2^{cre} Rictor$^{fl/fl}$ mice (B) or peripheral lymphocytes (C) from adult Rictor$^{fl/fl}$ and CD2^{cre} Rictor$^{fl/fl}$ mice were stimulated with rmIL-23 (10 ng/mL) plus rmIL-1β (10 ng/mL) for 15 min (n = 4–6/each group). *p*-Drp1 expression of CD3$^+$TCRγδ$^+$CD27$^-$ cells was examined by flow cytometry. Representative flow histograms and summarized *p*-Drp-1 MFI and fold increase are shown. MFI: mean fluorescent intensity.

(D) γδ T cells from peripheral lymphocytes of adult WT mice were cultured with Drp1 inhibitor Mdivi-1 at indicated concentrations for 24 h and stimulated with PMA/I plus Golgi-Plug for 5h (n = 4/each group). Intracellular IL-17/IFN-γ production by γδ T cells were analyzed by flow cytometry. Plots were gated on CD3$^+$TCRγδ$^+$ cells. Representative dot plots and summarized data are shown.

(E and F) WT mice were intraperitoneally injected with Mdivi-1 or DMSO (50 mg/kg) along with suitable carriers (5% Tween 80 and 40% PEG [polyethylene glycol]) starting Day 0 for 6 days (n = 5–9/each group). Mice were euthanized at Day 7 to harvest the peripheral LNs. Lymphocytes were stimulated with PMA/I plus Golgi-Plug for 5 h. Intracellular IL-17/IFN-γ (E) and transcription factors RORγt and c-Maf (F) were measured by flow cytometry. Plots were gated on CD3$^+$TCRγδ$^+$ cells. Representative dot plots and summarized data are shown. Data are representative of at least two independent experiments with similar results and are shown as mean ± SEM. Unpaired Student's *t* test (A–F) and Ordinary one-way ANOVA (B) were used. *p < 0.05, **p < 0.01, ****p < 0.0001; NS, not significant.

function, we treated γδ T cells from adult WT mice with ATP synthase inhibitor, oligomycin. Despite minimal cell death upon oligomycin treatment, cellular ATP levels (Figure 7B) and IL-17 production in γδ T cells (Figure 7C) were significantly reduced after oligomycin treatment. This finding led us to hypothesize that ATP might be the key metabolite that supports γδT17 commitment and effector function. To test this hypothesis, we reconstituted cellular ATP levels of γδ T cells using ATP vesicles (Vitasol) and control empty lipid vesicles (Con). Compared to control group, IL-17 production, c-Maf and RORγt expression were

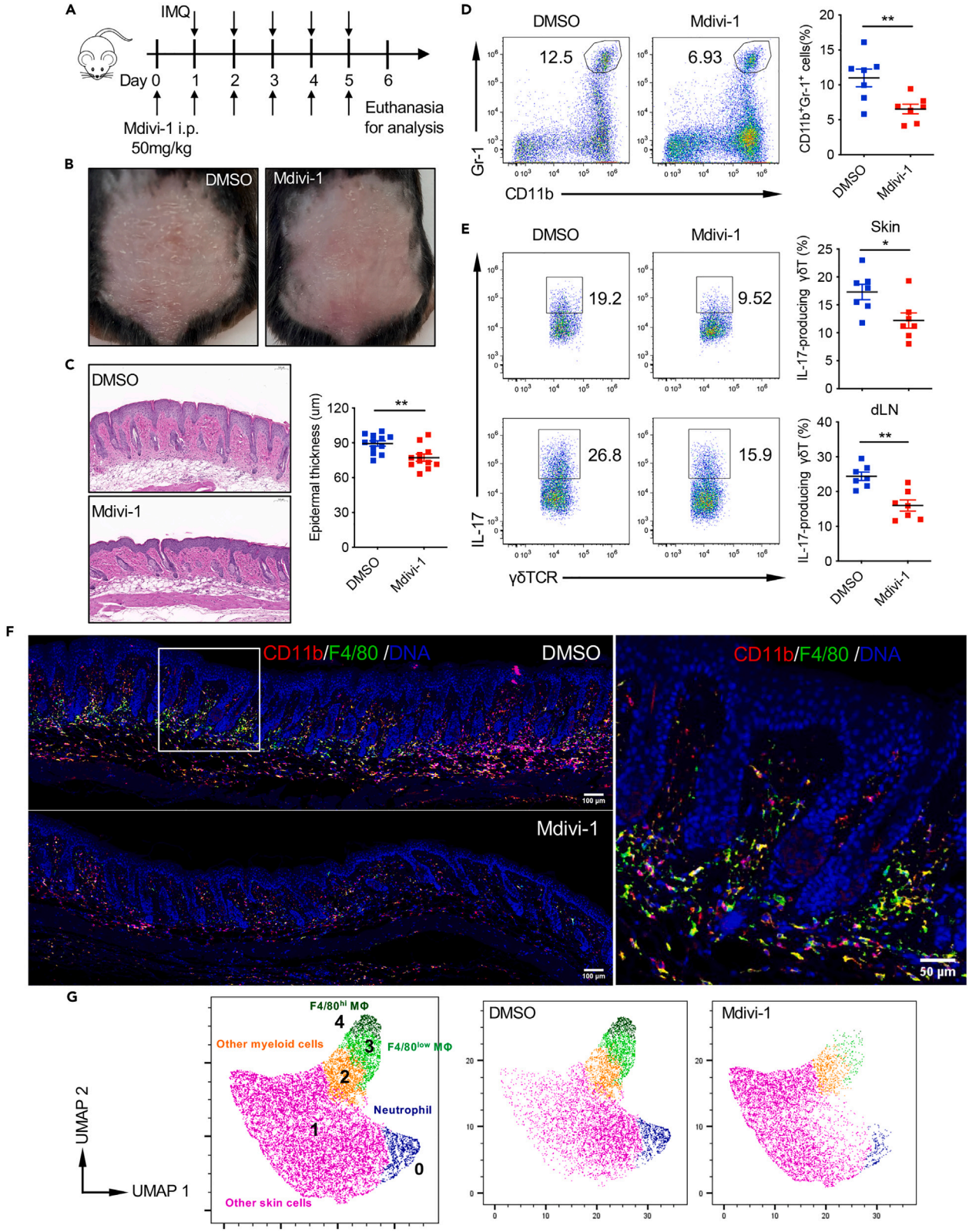
A
IMQ
Day 0 1 2 3 4 5 6
Mdivi-1 i.p.
50mg/kg
Euthanasia
for analysis
B
DMSO
Mdivi-1
C
DMSO
Mdivi-1
Epidermal thickness (um)
120
90
60
30
0
**
DMSO
Mdivi-1
D
DMSO
Mdivi-1
12.5
6.93
Gr-1
CD11b
CD11b+Gr-1+ cells(%)
20
15
10
5
0
**
DMSO
Mdivi-1
E
DMSO
Mdivi-1
19.2
9.52
26.8
15.9
IL-17
γδTCR
Skin
IL-17-producing γδT (%)
25
20
15
10
5
0
*
dLN
IL-17-producing γδT (%)
40
30
20
10
0
**
DMSO
Mdivi-1
F
CD11b/F4/80 /DNA
DMSO
Mdivi-1
100 μm
CD11b/F4/80 /DNA
50 μm
G
F4/80hi MΦ
4
Other myeloid cells
3
F4/80low MΦ
2
Neutrophil
1
0
Other skin cells
UMAP 2
UMAP 1
DMSO
Mdivi-1
20
10
0
0
10
20
30

Figure 6. Inhibition of Drp1 by Mdivi-1 alleviates IMQ-induced skin inflammation

(A) Treatment schema. WT mice were applied daily with topical IMQ cream for 5 days and received Mdivi-1 or DMSO (50 mg/kg, i.p.) treatment for 6 days.

(B) Representative gross images of back skin are shown.

(C) Representative H&E-stained skin sections are shown (n = 11–12/each group). Epidermal thickness at day 6 were measured. Scale bar, 100um.

(D and E) Skin single-cell suspensions were stained for CD11b/Gr-1 (D) and IL-17 production (E, top) without stimulation in γδ T cells (n = 7/each group). Cells from draining LN were stained for IL-17 production after stimulated with PMA/I plus Golgi-Plug for 5 h (E, bottom). Data are representative of two independent experiments with similar results. Data are shown as mean ± SEM. Unpaired Student's *t* test was used. *p < 0.05, **p < 0.01.

(F) Representative IMC images of skin sections stained with metal isotope labeled Abs against CD11b (red), F4/80 (green), and DNA (blue). Scale bars, 100um and 50um in magnification.

(G) UMAP analysis of the skin IMC images from DMSO or Mdivi-1 treated mice.

remarkably increased in a dose dependent manner in ATP vesicle-treated γδ T cells from E18 Rictor cKO thymus (Figures 7D and 7E) and adult Rictor cKO peripheral LNs (Figures S8A and S8B). Interestingly, ATP reconstitution further increased the IL-17 production of γδ T cells from WT fetal thymus (Figures S9A and S9B) and peripheral LNs (Figures S9C and S9D), indicating that cellular ATP level controls the function of γδT17 cells, no matter in metabolically impaired or intact state.

DISCUSSION

mTOR signaling pathway involves in T cell development, homeostasis, activation, and effector fate decision in physiological and pathological conditions.[29,30,41] mTORC1 coordinates its downstream HIF-1α to participate in Th17 differentiation.[42,43] In addition, mTORC1 deficiency leads to an impaired DN to DP transition in αβ T cell development but enhanced γδ T cell development.[44] However, mTORC1 is not required for thymic development of γδT17 cells as shown in the current study. In contrast, mTORC2 not only controls the effector function of γδT17 cells[40] but also embryonic γδT17 development and functional commitment as early as they emerge around E16. T cell progenitors undergo a highly dynamic process comprising discrete steps of lineage commitment in the thymus. mTORC2 deficiency results in accumulated $CD25^+CD27^+$ precursors, while $CD24^-CD27^-CD44^+$ mature γδ T cells and $CD24^+ROR\gamma t^+$ immature Vγ4 T cells are significantly decreased, suggesting that loss of Rictor hinders the process where γδ T cells should sequentially acquire IL-17-producing capability. Notably, mTORC2 selectively impacts the acquisition of γδ T effector function stage through regulating c-Maf expression, indicating that mTORC2 signaling is critical in γδT17 cell functional acquisition during development.

Recent studies have shown that γδT17 cells favor OXPHOS[27] and glutamine metabolism[40,45] over glycolysis, with strong mitochondrial activity and high expression of glutaminase (Gls) and glutamate dehydrogenase 1 (Glud1). The electron transport chain (ETC) drives oxidative phosphorylation in mitochondria to generate ATP and is composed of four protein complexes (complex I-IV), two electron carriers, and ATP synthase (complex V). Using scRNA-seq, c-Maf-expressing γδT17 clusters highly express genes related with complex I, IV, and V, confirming their high reliance on mitochondrial OXPHOS activity. Interestingly, γδT17 clusters also show higher expression of mitochondrial fission gene *Fis1*, providing preliminary evidence for the correlation between γδT17 effector function and mitochondrial fission. Despite the critical roles mTORC2 played in the γδT17 development, Rictor is expressed ubiquitously in all immune cells. This implies that the importance of the mTORC2 signaling pathway may vary in different immune cells. For example, there is hardly any evidence about mTORC2 on IFN-γ-producing γδT1 cells. In addition, mTORC2 activity is not required for the effector function of CD8 T cells, while it influences the memory generation and recall responses.[46,47] It also promotes the longevity of virus-specific memory CD4 T cells by preventing ferroptosis.[48] In the current study, we showed that Rictor regulates γδT17 development and effector function via Drp1-medaited mitochondrial fission. We believe that the reliance on Rictor-dependent ATP production causes the specific phenotype in γδT17 cell development.

mTOR signaling is closely related to mitochondrial dynamics.[36,49] Activation of mTOR signaling induces Drp-1-mediated mitochondrial fragmentation (fission) and thereby modulating natural killer (NK) cell antitumor activity under hypoxic tumor microenvironment.[49] The balance of mitochondrial fission and fusion is indispensably required in normal mitochondrial metabolic activity.[50,51] We found that γδ T cells deficient in mTORC2 possess lower $\Delta\Psi m$ and exhibit an impaired Drp1-mediated mitochondrial fission. This is revealed in γδ T cells from both fetal thymus and adult periphery tissues. Inhibition of Drp1 using small molecule inhibitor Mdivi-1 treatment abrogates IL-17 production in fetal thymic γδ T cells and adult peripheral γδ T cells. Transcriptional factors c-Maf and RORγt are concomitantly decreased in Mdivi-1-treated γδ T cells, suggesting that mTORC2/Drp-1/c-Maf axis is critical in the development and effector function of γδT17 cells. Additionally, Mdivi-1 treatment ameliorates IMQ-induced skin inflammation as a result of

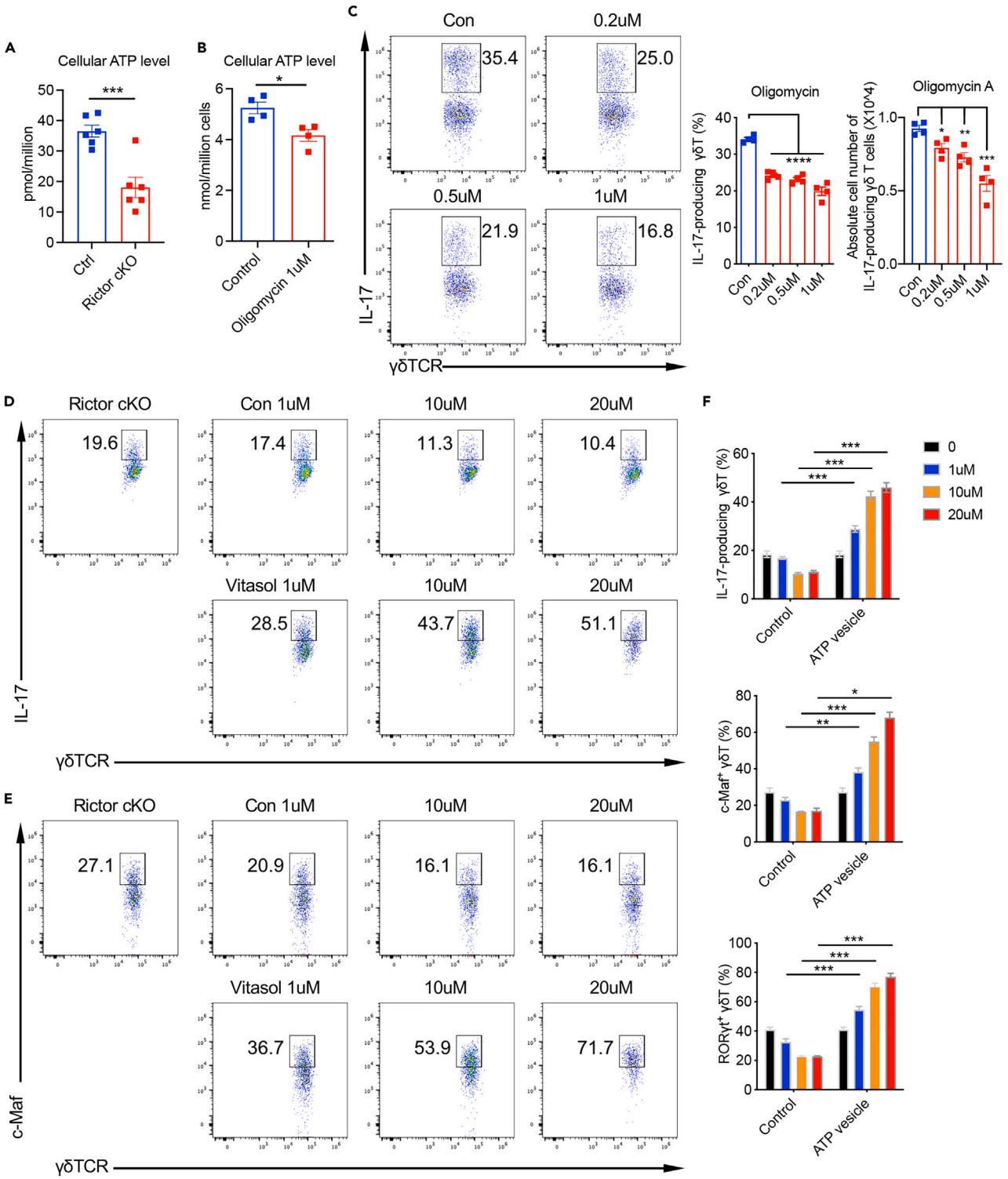

Figure 7. Reduced ATP level accounts for defective γδT17 in mTORC2 deficiency fetal thymus

(A) γδ T cells were sorted from E18 Rictor$^{fl/fl}$ and CD2^{cre} Rictor$^{fl/fl}$ fetal thymus. Cellular ATP levels were measured (n = 6/each group).

(B and C) γδ T cells were sorted from peripheral lymphocytes of adult WT mice and then cultured with vehicle and ATP synthase inhibitor oligomycin at indicated concentrations for 30 min (n = 4/each group). (B) Cellular ATP levels were measured. (C) Cells were then washed and stimulated with PMA/I for 5 h in the presence of Golgi-Plug. Intracellular IL-17/IFN-γ was measured by flow cytometry. Plots were gated on CD3$^+$TCRγδ$^+$ cells.

Figure 7. *Continued*

(D–F) Cells from E18 CD2^{cre} Rictor$^{fl/fl}$ fetal thymus were cultured with Control (Con) and ATP vesicles (Vitasol) at indicated concentrations in the presence of rmIL-23 (10 ng/mL) plus rmIL-1β (10 ng/mL) for 3 days and incubated with Golgi-Plug for 5 h (n = 4/each group). Intracellular IL-17 (D), c-Maf (E), and RORγt were measured by flow cytometry. Plots gated on CD3$^+$TCRγδ$^+$ cells cells. (F) Summarized percentages of IL-17$^+$/c-Maf$^+$/RORγt$^+$ γδ T cells were shown. Data are representative of at least two independent experiments with similar results and are shown as mean ± SEM. Unpaired Student's *t* test (A–C and F) and Mann-Whitney test (F: c-Maf data in 20uM group) were used. *p < 0.05, **p < 0.01, ***p < 0.001, ****p < 0.0001.

substantially reduced dermal γδT17 cells. Collectively, these findings suggest that mTORC2 may regulate γδT17 thymic commitment and functional acquisition through mitochondrial OXPHOS-mediated metabolic programming.

mTORC2 localizes in cytosolic mitochondria-associated endoplasmic reticulum (ER) membrane.[52,53] We showed that mTORC2 deficiency in fetal thymus leads to decreased c-Maf expression in γδ T cells. c-Maf cKO mice phenocopied mTORC2 cKO mice, at least for γδT17 development and functional acquisition. How does cytosolic mTORC2 modulate intranuclear transcription factor c-Maf expression? We found that mTORC2 deficiency in thymic and peripheral γδ T cells results in reduced intracellular ATP production, which is also causing defective IL-17 production. Although it is not surprising to observe lower ATP production in mTORC2-deficient γδ T cells, it is intriguing to examine whether reconstitution of ATP in fetal thymic mTORC2-deficient γδ T cells could restore their IL-17 production capability and regain their effector function.

ATP works as a form of metabolic currency that participates in cell differentiation, activation, and effector function.[54,55] ATP itself is cell membrane impermeable. Thus, its delivery into cells needs the help of additional reagents.[56] Previous studies used Streptolysin-O (SLO) to make pores in the cell membrane, so that ATP molecules can be delivered through pores.[57,58] Based on this delivery system, they reported that reduced ATP levels accounted for defects of PI3K-Akt-Foxo1 signaling in LDHA-deficient CD4 and CD8 T cells. However, SLO-induced membrane pores also result in the loss of cellular components, which probably impacts cellular metabolism in an unknown way. In this study, we used an ATP-encapsulated liposome[59–61] to restore intracellular ATP levels in mTORC2 deficient γδ T cells through membrane fusion. We showed that reconstitution of ATP in mTORC2-deficient γδ T cells fully restored IL-17 production with increased c-Maf and RORγt expression, suggesting that ATP may function as a metabolite directly interacting with transcription factors essential for γδT17 functional acquisition during development. Notably, exogenous ATP infusion also substantially increases IL-17 production in WT γδ T cells, suggesting that intracellular ATP may play a critical role in reprogramming γδT17 cells in the periphery. Although it is unknown how ATP directly regulates transcription factors, ATP probably exerts a trophic effect to support these signaling requirements and transcriptional factor expression. Transcription is the first step of gene expression, which is initiated by the recognition of RNA polymerase to the DNA promoter region. ATP has been reported to be indispensable in transcription initiation by RNA polymerase II.[62,63] It is likely that ATP fuels RNA polymerase to bind to the c-Maf promoter region and in turn enhances c-Maf expression during γδ T functional commitment stage, therefore facilitating γδT17 development. Alternatively, ATP may participate in c-Maf translation and post-translational modification. A previous study showed that PI3Kδ functions as an ATP sensor that is sensitive to the fluctuation of cellular energy state, thereby building a bridge between cellular energy and transcriptional factor Foxo1.[57] Thus, it is possible that mTORC2 may regulate ATP sensor in γδT17 cells that connects cellular energy with c-Maf expression. The detailed molecular mechanism needs further investigation.

Limitations of the study

It is worth noting that due to the limited cell number of γδ T cells in the fetal thymus, we performed some *in vitro* manipulations, such as viral transduction and Mdivi-1/Oligomycin treatment, with γδ T cells from adult peripheral LNs. Given the potential differences between fetal and adult populations in these experiments, the establishment of the FTOC system and the use of CD2-Cre; Drp1$^{fl/fl}$ cKO mice will be considered in our future study. In addition, we showed that intracellular ATP supported the function of γδT17 cells. Further study is needed to determine the molecular mechanism by which ATP facilitates the expression of transcription factor c-Maf.

STAR★METHODS

Detailed methods are provided in the online version of this paper and include the following:

- KEY RESOURCES TABLE
- RESOURCE AVAILABILITY
  - Lead contact
  - Materials availability

SUPPLEMENTAL INFORMATION

Supplemental information can be found online at https://doi.org/10.1016/j.isci.2023.106630.

ACKNOWLEDGMENTS

Funding: This work was partly supported by the NIH RO1AI128818 and RO1CA161198 (J.Y). The IMC was performed in the Functional Immunomics Core supported by the NIH P20GM135004.

AUTHOR CONTRIBUTIONS

Conceptualization: Y.W., H.Q., and J.Y. Methodology: Y.W., H.Q., Y.C., X.C., H.L., D.E.M., C.D., X.H., J.H.C., and H.S. Investigation: Y.W., H.Q., Y.C., X.C., H.L., D.E.M., C.D., X.H., J.H.C., H.S., S.C., E.C.R., H.Z., J.Z., and F.Q. Funding acquisition and supervision: J.Y. Writing – original draft: Y.W. and J.Y. Writing – review & editing: Y.W., J.H.C., E.C.R., S.C., and J.Y.

DECLARATION OF INTERESTS

Authors declare that they have no competing interests.

Received: July 20, 2022
Revised: February 17, 2023
Accepted: April 4, 2023
Published: April 10, 2023

REFERENCES

1. Jensen, K.D.C., Su, X., Shin, S., Li, L., Youssef, S., Yamasaki, S., Steinman, L., Saito, T., Locksley, R.M., Davis, M.M., et al. (2008). Thymic selection determines gammadelta T cell effector fate: antigen-naive cells make interleukin-17 and antigen-experienced cells make interferon gamma. Immunity *29*, 90–100. https://doi.org/10.1016/j.immuni.2008.04.022.

2. Haas, J.D., Ravens, S., Düber, S., Sandrock, I., Oberdörfer, L., Kashani, E., Chennupati, V., Föhse, L., Naumann, R., Weiss, S., et al. (2012). Development of interleukin-17-producing gammadelta T cells is restricted to a functional embryonic wave. Immunity *37*, 48–59. https://doi.org/10.1016/j.immuni.2012.06.003.

3. Prinz, I., Silva-Santos, B., and Pennington, D.J. (2013). Functional development of gammadelta T cells. Eur. J. Immunol. *43*, 1988–1994. https://doi.org/10.1002/eji.201343759.

4. Heilig, J.S., and Tonegawa, S. (1986). Diversity of murine gamma genes and expression in fetal and adult T lymphocytes. Nature *322*, 836–840. https://doi.org/10.1038/322836a0.

5. Rei, M., Gonçalves-Sousa, N., Lança, T., Thompson, R.G., Mensurado, S., Balkwill, F.R., Kulbe, H., Pennington, D.J., and Silva-Santos, B. (2014). Murine CD27(-) Vgamma6(+) gammadelta T cells producing IL-17A promote ovarian cancer growth via mobilization of protumor small peritoneal macrophages. Proc. Natl. Acad. Sci. USA *111*, E3562–E3570. https://doi.org/10.1073/pnas.1403424111.

6. Coffelt, S.B., Kersten, K., Doornebal, C.W., Weiden, J., Vrijland, K., Hau, C.S., Verstegen, N.J.M., Ciampricotti, M., Hawinkels, L.J.A.C., Jonkers, J., and de Visser, K.E. (2015). IL-17-producing gammadelta T cells and neutrophils conspire to promote breast cancer metastasis. Nature *522*, 345–348. https://doi.org/10.1038/nature14282.

7. Wu, P., Wu, D., Ni, C., Ye, J., Chen, W., Hu, G., Wang, Z., Wang, C., Zhang, Z., Xia, W., et al. (2014). gammadeltaT17 cells promote the accumulation and expansion of myeloid-derived suppressor cells in human colorectal cancer. Immunity *40*, 785–800. https://doi.org/10.1016/j.immuni.2014.03.013.

8. Cai, Y., Shen, X., Ding, C., Qi, C., Li, K., Li, X., Jala, V.R., Zhang, H.G., Wang, T., Zheng, J., and Yan, J. (2011). Pivotal role of dermal IL-17-producing gammadelta T cells in skin inflammation. Immunity *35*, 596–610. https://doi.org/10.1016/j.immuni.2011.08.001.

9. Ribot, J.C., Lopes, N., and Silva-Santos, B. (2021). Gammadelta T cells in tissue physiology and surveillance. Nat. Rev. Immunol. *21*, 221–232. https://doi.org/10.1038/s41577-020-00452-4.

10. Sumaria, N., Grandjean, C.L., Silva-Santos, B., and Pennington, D.J. (2017). Strong TCRgammadelta signaling prohibits thymic development of IL-17a-secreting gammadelta T cells. Cell Rep. *19*, 2469–2476. https://doi.org/10.1016/j.celrep.2017.05.071.

11. Turchinovich, G., and Hayday, A.C. (2011). Skint-1 identifies a common molecular mechanism for the development of interferon-gamma-secreting versus interleukin-17-secreting gammadelta T cells. Immunity *35*, 59–68. https://doi.org/10.1016/j.immuni.2011.04.018.

12. Fahl, S.P., Coffey, F., Kain, L., Zarin, P., Dunbrack, R.L., Jr., Teyton, L., Zúñiga-Pflücker, J.C., Kappes, D.J., and Wiest, D.L. (2018). Role of a selecting ligand in shaping the murine gammadelta-TCR repertoire. Proc. Natl. Acad. Sci. USA *115*, 1889–1894. https://doi.org/10.1073/pnas.1718328115.

13. Muñoz-Ruiz, M., Ribot, J.C., Grosso, A.R., Gonçalves-Sousa, N., Pamplona, A., Pennington, D.J., Regueiro, J.R., Fernández-Malavé, E., and Silva-Santos, B. (2016). TCR signal strength controls thymic differentiation

of discrete proinflammatory gammadelta T cell subsets. Nat. Immunol. *17*, 721–727. https://doi.org/10.1038/ni.3424.

14. Wencker, M., Turchinovich, G., Di Marco Barros, R., Deban, L., Jandke, A., Cope, A., and Hayday, A.C. (2014). Innate-like T cells straddle innate and adaptive immunity by altering antigen-receptor responsiveness. Nat. Immunol. *15*, 80–87. https://doi.org/10.1038/ni.2773.

15. Malhotra, N., Narayan, K., Cho, O.H., Sylvia, K.E., Yin, C., Melichar, H., Rashighi, M., Lefebvre, V., Harris, J.E., Berg, L.J., et al. (2013). A network of high-mobility group box transcription factors programs innate interleukin-17 production. Immunity *38*, 681–693. https://doi.org/10.1016/j.immuni.2013.01.010.

16. In, T.S.H., Trotman-Grant, A., Fahl, S., Chen, E.L.Y., Zarin, P., Moore, A.J., Wiest, D.L., Zuniga-Pflucker, J.C., and Anderson, M.K. (2017). HEB is required for the specification of fetal IL-17-producing gammadelta T cells. Nat. Commun. *8*, 2004. https://doi.org/10.1038/s41467-017-02225-5.

17. Spidale, N.A., Sylvia, K., Narayan, K., Miu, B., Frascoli, M., Melichar, H.J., Zhihao, W., Kisielow, J., Palin, A., Serwold, T., et al. (2018). Interleukin-17-Producing gammadelta T Cells originate from SOX13(+) progenitors that are independent of gammadeltaTCR signaling. Immunity *49*, 857–872.e5. https://doi.org/10.1016/j.immuni.2018.09.010.

18. Zuberbuehler, M.K., Parker, M.E., Wheaton, J.D., Espinosa, J.R., Salzler, H.R., Park, E., and Ciofani, M. (2019). The transcription factor c-Maf is essential for the commitment of IL-17-producing gammadelta T cells. Nat. Immunol. *20*, 73–85. https://doi.org/10.1038/s41590-018-0274-0.

19. Sagar, Pokrovskii, M., Herman, J.S., Naik, S., Sock, E., Zeis, P., Lausch, U., Wegner, M., Tanriver, Y., Littman, D.R., and Grün, D. (2020). Deciphering the regulatory landscape of fetal and adult gammadelta T-cell development at single-cell resolution. EMBO J. *39*, e104159. https://doi.org/10.15252/embj.2019104159.

20. Lu, Y., Cao, X., Zhang, X., and Kovalovsky, D. (2015). PLZF controls the development of fetal-derived IL-17+Vgamma6+ gammadelta T cells. J. Immunol. *195*, 4273–4281. https://doi.org/10.4049/jimmunol.1500939.

21. Fahl, S.P., Contreras, A.V., Verma, A., Qiu, X., Harly, C., Radtke, F., Zúñiga-Pflücker, J.C., Murre, C., Xue, H.H., Sen, J.M., and Wiest, D.L. (2021). The E protein-TCF1 axis controls gammadelta T cell development and effector fate. Cell Rep. *34*, 108716. https://doi.org/10.1016/j.celrep.2021.108716.

22. Do, J.S., Fink, P.J., Li, L., Spolski, R., Robinson, J., Leonard, W.J., Letterio, J.J., and Min, B. (2010). Cutting edge: spontaneous development of IL-17-producing gamma delta T cells in the thymus occurs via a TGF-beta 1-dependent mechanism. J. Immunol. *184*, 1675–1679. https://doi.org/10.4049/jimmunol.0903539.

23. Shibata, K., Yamada, H., Sato, T., Dejima, T., Nakamura, M., Ikawa, T., Hara, H., Yamasaki, S., Kageyama, R., Iwakura, Y., et al. (2011). Notch-Hes1 pathway is required for the development of IL-17-producing gammadelta T cells. Blood *118*, 586–593. https://doi.org/10.1182/blood-2011-02-334995.

24. Dienz, O., DeVault, V.L., Musial, S.C., Mistri, S.K., Mei, L., Baraev, A., Dragon, J.A., Krementsov, D., Veillette, A., and Boyson, J.E. (2020). Critical role for SLAM/SAP signaling in the thymic developmental programming of IL-17- and IFN-gamma-Producing gammadelta T cells. J. Immunol. *204*, 1521–1534. https://doi.org/10.4049/jimmunol.1901082.

25. Sumaria, N., Martin, S., and Pennington, D.J. (2021). Constrained TCRγδ-associated Syk activity engages PI3K to facilitate thymic development of IL-17A-secreting γδ T cells. Sci. Signal. *14*, eabc5884. https://doi.org/10.1126/scisignal.abc5884.

26. Zhang, Y., Chen, Y., Ma, R., Jiang, Y., Liu, J., Lin, Y., Chen, S., Xia, M., Zou, F., Zhang, J., et al. (2020). UHRF1 controls thymocyte fate decisions through the epigenetic regulation of EGR1 expression. J. Immunol. *204*, 3248–3261. https://doi.org/10.4049/jimmunol.1901471.

27. Lopes, N., McIntyre, C., Martin, S., Raverdeau, M., Sumaria, N., Kohlgruber, A.C., Fiala, G.J., Agudelo, L.Z., Dyck, L., Kane, H., et al. (2021). Distinct metabolic programs established in the thymus control effector functions of gammadelta T cell subsets in tumor microenvironments. Nat. Immunol. *22*, 179–192. https://doi.org/10.1038/s41590-020-00848-3.

28. Cai, Y., Xue, F., Qin, H., Chen, X., Liu, N., Fleming, C., Hu, X., Zhang, H.G., Chen, F., Zheng, J., and Yan, J. (2019). Differential roles of the mTOR-STAT3 signaling in dermal gammadelta T cell effector function in skin inflammation. Cell Rep. *27*, 3034–3048.e5. https://doi.org/10.1016/j.celrep.2019.05.019.

29. Chi, H. (2012). Regulation and function of mTOR signalling in T cell fate decisions. Nat. Rev. Immunol. *12*, 325–338. https://doi.org/10.1038/nri3198.

30. Huang, H., Long, L., Zhou, P., Chapman, N.M., and Chi, H. (2020). mTOR signaling at the crossroads of environmental signals and T-cell fate decisions. Immunol. Rev. *295*, 15–38. https://doi.org/10.1111/imr.12845.

31. Liu, G.Y., and Sabatini, D.M. (2020). mTOR at the nexus of nutrition, growth, ageing and disease. Nat. Rev. Mol. Cell Biol. *21*, 183–203. https://doi.org/10.1038/s41580-019-0199-y.

32. Yang, Q., Liu, X., Liu, Q., Guan, Z., Luo, J., Cao, G., Cai, R., Li, Z., Xu, Y., Wu, Z., et al. (2020). Roles of mTORC1 and mTORC2 in controlling gammadelta T1 and gammadelta T17 differentiation and function. Cell Death Differ. *27*, 2248–2262. https://doi.org/10.1038/s41418-020-0500-9.

33. Ribot, J.C., deBarros, A., Pang, D.J., Neves, J.F., Peperzak, V., Roberts, S.J., Girardi, M., Borst, J., Hayday, A.C., Pennington, D.J., and Silva-Santos, B. (2009). CD27 is a thymic determinant of the balance between interferon-gamma- and interleukin 17-producing gammadelta T cell subsets. Nat. Immunol. *10*, 427–436. https://doi.org/10.1038/ni.1717.

34. Vantourout, P., and Hayday, A. (2013). Six-of-the-best: unique contributions of gammadelta T cells to immunology. Nat. Rev. Immunol. *13*, 88–100. https://doi.org/10.1038/nri3384.

35. van der Bliek, A.M., Shen, Q., and Kawajiri, S. (2013). Mechanisms of mitochondrial fission and fusion. Cold Spring Harbor Perspect. Biol. *5*, a011072. https://doi.org/10.1101/cshperspect.a011072.

36. Morita, M., Prudent, J., Basu, K., Goyon, V., Katsumura, S., Hulea, L., Pearl, D., Siddiqui, N., Strack, S., McGuirk, S., et al. (2017). mTOR controls mitochondrial dynamics and cell survival via MTFP1. Mol. Cell *67*, 922–935.e5. https://doi.org/10.1016/j.molcel.2017.08.013.

37. Han, Y., Mora, J., Huard, A., da Silva, P., Wiechmann, S., Putyrski, M., Schuster, C., Elwakeel, E., Lang, G., Scholz, A., et al. (2019). IL-38 ameliorates skin inflammation and limits IL-17 production from gammadelta T cells. Cell Rep. *27*, 835–846.e5. https://doi.org/10.1016/j.celrep.2019.03.082.

38. Liu, S., Liu, S., He, B., Li, L., Li, L., Wang, J., Cai, T., Chen, S., and Jiang, H. (2021). OXPHOS deficiency activates global adaptation pathways to maintain mitochondrial membrane potential. EMBO Rep. *22*, e51606. https://doi.org/10.15252/embr.202051606.

39. Bhatti, J.S., Bhatti, G.K., and Reddy, P.H. (2017). Mitochondrial dysfunction and oxidative stress in metabolic disorders - a step towards mitochondria based therapeutic strategies. Biochim. Biophys. Acta, Mol. Basis Dis. *1863*, 1066–1077. https://doi.org/10.1016/j.bbadis.2016.11.010.

40. Chen, X., Cai, Y., Hu, X., Ding, C., He, L., Zhang, X., Chen, F., and Yan, J. (2022). Differential metabolic requirement governed by transcription factor c-Maf dictates innate gammadeltaT17 effector functionality in mice and humans. Sci. Adv. *8*, eabm9120. https://doi.org/10.1126/sciadv.abm9120.

41. Werlen, G., Jain, R., and Jacinto, E. (2021). MTOR signaling and metabolism in early T cell development. Genes *12*, 728. https://doi.org/10.3390/genes12050728.

42. Corcoran, S.E., and O'Neill, L.A.J. (2016). HIF1alpha and metabolic reprogramming in inflammation. J. Clin. Invest. *126*, 3699–3707. https://doi.org/10.1172/JCI84431.

43. Dang, E.V., Barbi, J., Yang, H.Y., Jinasena, D., Yu, H., Zheng, Y., Bordman, Z., Fu, J., Kim, Y., Yen, H.R., et al. (2011). Control of T(H)17/T(reg) balance by hypoxia-inducible factor 1. Cell *146*, 772–784. https://doi.org/10.1016/j.cell.2011.07.033.

44. Yang, K., Blanco, D.B., Chen, X., Dash, P., Neale, G., Rosencrance, C., Easton, J., Chen, W., Cheng, C., Dhungana, Y., et al. (2018). Metabolic signaling directs the reciprocal lineage decisions of alphabeta and gammadelta T cells. Sci. Immunol. *3*, eaas9818. https://doi.org/10.1126/sciimmunol.aas9818.

45. Li, G., Liu, L., Yin, Z., Ye, Z., and Shen, N. (2021). Glutamine metabolism is essential for the production of IL-17A in gammadelta T cells and skin inflammation. Tissue Cell *71*, 101569. https://doi.org/10.1016/j.tice.2021.101569.

46. Pollizzi, K.N., Patel, C.H., Sun, I.H., Oh, M.H., Waickman, A.T., Wen, J., Delgoffe, G.M., and Powell, J.D. (2015). mTORC1 and mTORC2 selectively regulate CD8(+) T cell differentiation. J. Clin. Invest. *125*, 2090–2108. https://doi.org/10.1172/JCI77746.

47. Zhang, L., Tschumi, B.O., Lopez-Mejia, I.C., Oberle, S.G., Meyer, M., Samson, G., Rüegg, M.A., Hall, M.N., Fajas, L., Zehn, D., et al. (2016). Mammalian target of rapamycin complex 2 controls CD8 T cell memory differentiation in a foxo1-dependent manner. Cell Rep. *14*, 1206–1217. https://doi.org/10.1016/j.celrep.2015.12.095.

48. Wang, Y., Tian, Q., Hao, Y., Yao, W., Lu, J., Chen, C., Chen, X., Lin, Y., Huang, Q., Xu, L., et al. (2022). The kinase complex mTORC2 promotes the longevity of virus-specific memory CD4(+) T cells by preventing ferroptosis. Nat. Immunol. *23*, 303–317. https://doi.org/10.1038/s41590-021-01090-1.

49. Zheng, X., Qian, Y., Fu, B., Jiao, D., Jiang, Y., Chen, P., Shen, Y., Zhang, H., Sun, R., Tian, Z., and Wei, H. (2019). Mitochondrial fragmentation limits NK cell-based tumor immunosurveillance. Nat. Immunol. *20*, 1656–1667. https://doi.org/10.1038/s41590-019-0511-1.

50. Liesa, M., and Shirihai, O.S. (2013). Mitochondrial dynamics in the regulation of nutrient utilization and energy expenditure. Cell Metabol. *17*, 491–506. https://doi.org/10.1016/j.cmet.2013.03.002.

51. Buck, M.D., O'Sullivan, D., Klein Geltink, R.I., Curtis, J.D., Chang, C.H., Sanin, D.E., Qiu, J., Kretz, O., Braas, D., van der Windt, G.J.W., et al. (2016). Mitochondrial dynamics controls T cell fate through metabolic programming. Cell *166*, 63–76. https://doi.org/10.1016/j.cell.2016.05.035.

52. Betz, C., Stracka, D., Prescianotto-Baschong, C., Frieden, M., Demaurex, N., and Hall, M.N. (2013). Feature Article: mTOR complex 2-Akt signaling at mitochondria-associated endoplasmic reticulum membranes (MAM) regulates mitochondrial physiology. Proc. Natl. Acad. Sci. USA *110*, 12526–12534. https://doi.org/10.1073/pnas.1302455110.

53. Zinzalla, V., Stracka, D., Oppliger, W., and Hall, M.N. (2011). Activation of mTORC2 by association with the ribosome. Cell *144*, 757–768. https://doi.org/10.1016/j.cell.2011.02.014.

54. Pearce, E.L., Poffenberger, M.C., Chang, C.H., and Jones, R.G. (2013). Fueling immunity: insights into metabolism and lymphocyte function. Science *342*, 1242454. https://doi.org/10.1126/science.1242454.

55. Geltink, R.I.K., Kyle, R.L., and Pearce, E.L. (2018). Unraveling the complex interplay between T cell metabolism and function. Annu. Rev. Immunol. *36*, 461–488. https://doi.org/10.1146/annurev-immunol-042617-053019.

56. Walev, I., Bhakdi, S.C., Hofmann, F., Djonder, N., Valeva, A., Aktories, K., and Bhakdi, S. (2001). Delivery of proteins into living cells by reversible membrane permeabilization with streptolysin-O. Proc. Natl. Acad. Sci. USA *98*, 3185–3190. https://doi.org/10.1073/pnas.051429498.

57. Xu, K., Yin, N., Peng, M., Stamatiades, E.G., Chhangawala, S., Shyu, A., Li, P., Zhang, X., Do, M.H., Capistrano, K.J., et al. (2021). Glycolytic ATP fuels phosphoinositide 3-kinase signaling to support effector T helper 17 cell responses. Immunity *54*, 976–987.e7. https://doi.org/10.1016/j.immuni.2021.04.008.

58. Xu, K., Yin, N., Peng, M., Stamatiades, E.G., Shyu, A., Li, P., Zhang, X., Do, M.H., Wang, Z., Capistrano, K.J., et al. (2021). Glycolysis fuels phosphoinositide 3-kinase signaling to bolster T cell immunity. Science *371*, 405–410. https://doi.org/10.1126/science.abb2683.

59. Mo, Y., Sarojini, H., Wan, R., Zhang, Q., Wang, J., Eichenberger, S., Kotwal, G.J., and Chien, S. (2019). Intracellular ATP delivery causes rapid tissue regeneration via upregulation of cytokines, chemokines, and stem cells. Front. Pharmacol. *10*, 1502. https://doi.org/10.3389/fphar.2019.01502.

60. Sarojini, H., Bajorek, A., Wan, R., Wang, J., Zhang, Q., Billeter, A.T., and Chien, S. (2021). Enhanced skin incisional wound healing with intracellular ATP delivery via macrophage proliferation and direct collagen production. Front. Pharmacol. *12*, 594586. https://doi.org/10.3389/fphar.2021.594586.

61. Chien, S. (2010). Intracellular ATP delivery using highly fusogenic liposomes. Methods Mol. Biol. *605*, 377–391. https://doi.org/10.1007/978-1-60327-360-2_26.

62. Bunick, D., Zandomeni, R., Ackerman, S., and Weinmann, R. (1982). Mechanism of RNA polymerase II–specific initiation of transcription in vitro: ATP requirement and uncapped runoff transcripts. Cell *29*, 877–886. https://doi.org/10.1016/0092-8674(82)90449-4.

63. Serizawa, H., Tsuchihashi, Z., and Mizumoto, K. (1997). The RNA polymerase II preinitiation complex formed in the presence of ATP. Nucleic Acids Res. *25*, 4079–4084. https://doi.org/10.1093/nar/25.20.4079.

64. Stuart, T., Butler, A., Hoffman, P., Hafemeister, C., Papalexi, E., Mauck, W.M., III, Hao, Y., Stoeckius, M., Smibert, P., and Satija, R. (2019). Comprehensive integration of single-cell data. Cell *177*, 1888–1902.e21.

65. Liu, M., Tong, Z., Ding, C., Luo, F., Wu, S., Wu, C., Albeituni, S., He, L., Hu, X., Tieri, D., et al. (2020). Transcription factor c-Maf is a checkpoint that programs macrophages in lung cancer. J. Clin. Invest. *130*, 2081–2096. https://doi.org/10.1172/JCI131335.

66. Andrews, S. (2015). FastQC: A Quality Control Tool for High Throughput Sequence Data.

67. Lun, A.T.L., Riesenfeld, S., Andrews, T., Dao, T.P., Gomes, T.; Participants in the 1st Human Cell Atlas Jamboree, and Marioni, J.C. (2019). EmptyDrops: distinguishing cells from empty droplets in droplet-based single-cell RNA sequencing data. Genome Biol. *20*, 63–69.

68. Hafemeister, C., and Satija, R. (2019). Normalization and variance stabilization of single-cell RNA-seq data using regularized negative binomial regression. Genome Biol. *20*, 296–315.

69. Becht, E., McInnes, L., Healy, J., Dutertre, C.-A., Kwok, I.W.H., Ng, L.G., Ginhoux, F., and Newell, E.W. (2019). Dimensionality reduction for visualizing single-cell data using UMAP. Nat. Biotechnol. *37*, 38–44.

70. Diaz-Mejia, J.J., Meng, E.C., Pico, A.R., MacParland, S.A., Ketela, T., Pugh, T.J., Bader, G.D., and Morris, J.H. (2019). Evaluation of methods to assign cell type labels to cell clusters from single-cell RNA-sequencing data. F1000Research *8*. https://doi.org/10.12688/f1000research.18490.1.

71. Hänzelmann, S., Castelo, R., and Guinney, J. (2013). GSVA: gene set variation analysis for microarray and RNA-seq data. BMC Bioinf. *14*, 7.

72. Finak, G., McDavid, A., Yajima, M., Deng, J., Gersuk, V., Shalek, A.K., Slichter, C.K., Miller, H.W., McElrath, M.J., Prlic, M., et al. (2015). MAST: a flexible statistical framework for assessing transcriptional changes and characterizing heterogeneity in single-cell RNA sequencing data. Genome Biol. *16*, 278–313.

73. Cai, Y., Xue, F., Fleming, C., Yang, J., Ding, C., Ma, Y., Liu, M., Zhang, H.G., Zheng, J., Xiong, N., and Yan, J. (2014). Differential developmental requirement and peripheral regulation for dermal Vgamma4 and Vgamma6T17 cells in health and inflammation. Nat. Commun. *5*, 3986. https://doi.org/10.1038/ncomms4986.

STAR★METHODS

KEY RESOURCES TABLE

REAGENT or RESOURCE	SOURCE	IDENTIFIER
Antibodies		
Anti-mouse CD3 Percp/Cy5.5 (clone 17A2)	Biolegend	Cat#100218
Anti-mouse CD3 PE/Cy7 (clone 17A2)	Biolegend	Cat#100220
Anti-mouse CD3 APC/Cy7 (clone 17A2)	Biolegend	Cat#100222
Anti-mouse CD3 PE (clone 17A2)	Biolegend	Cat#100206
Anti-mouse γδTCR APC (clone GL3)	Biolegend	Cat#118116
Anti-mouse γδTCR Percp/Cy5.5 (clone GL3)	Biolegend	Cat#118118
Anti-mouse γδTCR PE/Cy7 (clone GL3)	Biolegend	Cat#118124
Anti-mouse CD4 FITC (clone GK1.5)	Biolegend	Cat#100406
Anti-mouse CD8 APC (clone 53-6.7)	Biolegend	Cat#100712
Anti-mouse CD8 Percp (clone 53-6.7)	Biolegend	Cat#100732
Anti-mouse CD27 FITC (clone LG.3A10)	Biolegend	Cat#124208
Anti-mouse CD27 PE/Cy7 (clone LG.3A10)	Biolegend	Cat#124216
Anti-mouse Vγ4 FITC (clone UC3-10A6)	Biolegend	Cat#137704
Anti-mouse Vγ4 PE (clone UC3-10A6)	Biolegend	Cat#137705
Anti-mouse Vγ4 APC (clone UC3-10A6)	Biolegend	Cat#137708
Anti-mouse Vγ6 (clone 17D1)	Dr. Tigelaar (Department of Dermatology, Yale university)	N/A
Anti-mouse Vγ5 APC (clone 536)	Biolegend	Cat#137506
Anti-mouse IL-17A PE/Cy7 (clone TC11-18H10.1)	Biolegend	Cat#506922
Anti-mouse IFN-γ PE (clone XMG1.2)	Biolegend	Cat#505808
Anti-mouse RORγt Percp/Cy5.5 (clone Q31-378)	BD Biosciences	Cat#562683
Anti-mouse RORγt PE (clone AFXJS-9)	eBioscience	Cat#12-6988-82
Anti-mouse c-Maf PE (clone sym0F1)	eBioscience	Cat#12-9855-42
Anti-mouse CD44 PE (clone IM7)	eBioscience	Cat#12-0441-82
Anti-mouse CD25 APC (clone 3C7)	Biolegend	Cat#101910
Anti-mouse CD24 PE (clone M1/69)	eBioscience	Cat#12-0242-82
Anti-mouse CD24 Percp/Cy5.5 (clone M1/69)	Biolegend	Cat#101824
Anti-mouse CD73 (clone TY/11.8)	Biolegend	Cat#127224
Anti-mouse Thy-1.2 APC/Cy7 (clone 30-H12)	Biolegend	Cat#105328
Anti-rat IgM FITC (clone MRM-47)	Biolegend	Cat#408905
Anti-rabbit IgG PE (clone Poly4064)	Biolegend	Cat#406421
Rat IgG1 isotype antibody PE (clone RTK2071)	Biolegend	Cat#400408
Rat IgG1 isotype antibody PE/Cy7 (clone RTK2071)	Biolegend	Cat#400416
Mouse IgG2b isotype antibody PE (clone MPC-11)	Biolegend	Cat#400312
Phospho-DRP1 (Ser616) Antibody	Cell Signaling Technology	Cat#3455S
Fixable Viability Dye eFluor™ 780	eBioscience	Cat#65-0865-14
Anti-Hu/Ms CD11b (EPR1344)-146Nd	Fluidigm	Cat#91H007146
Anti-Mouse Ly-6G (1A8)-141Pr	Fluidigm	Cat#3141008B
Anti-F4/80 (D2S9R)-166Er	Fluidigm	Cat# 91H030166
Ultra-LEAF™ Purified anti-mouse CD3ε Antibody (clone 145-2C11)	Biolegend	Cat#100340

(*Continued on next page*)

Continued

REAGENT or RESOURCE	SOURCE	IDENTIFIER
anti-mouse γδTCR (clone UC7)	Home made	N/A
Bacterial and virus strains		
MAF Lentivirus (Mouse) (CMV) (pLenti-GIII-CMV-GFP-2A-Puro)	Applied Biological Materials	278970640396
Lenti-CMV-GFP-2A-Puro-Blank Lentivirus	Applied Biological Materials	LVP690
Chemicals, peptides, and recombinant proteins		
Fetal Bovine Serum	Atlanta Biologicals	Cat#SIII50
HEPES	Corning	Cat#25-060-CI
RPMI 1640	Sigma-Aldrich	Cat#R8758
Dulbecco's Phosphate Buffered Saline (PBS)	Sigma-Aldrich	Cat#D8537
Aldara (5% Imiquimod)	3M Pharmaceuticals	N/A
Bovine Serum Albumin	Equitech-Bio	Cat#BAC62-1000
Tetramethylrhodamine, Methyl Ester, Perchlorate (TMRM)	Thermo Scientific	Cat#M20036
Phorbol 12-myristate 13-acetate (PMA)	Sigma-Aldrich	Cat#P8139
Ionomycin	EMD Millipore Corp	Cat#407952
Brefeldin A (1000X)	Biolegend	Cat#420601
Fixation Buffer	Biolegend	Cat#420801
Intracellular Staining Permeabilization Wash Buffer (10X)	Biolegend	Cat#421002
Methanol	Fischer Chemical	Cat#A412-1
Formaldehyde	Polysciences, Inc	Cat#04018
Mitochondrial Division Inhibitor (Mdivi-1)	Sigma-Aldrich	Cat#M0199
Oligomycin A	Sigma-Aldrich	Cat#75351
Polybrene	Santa Cruz	Cat#sc-134220
Antigen Retrieval Buffer	Abcam	Cat#ab93684
Dulbecco's Phosphate Buffered Saline (DPBS)	Sigma-Aldrich	Cat#D8537
Intercalator-Ir	Fluidigm	Cat#201192A
Vitasol liposome/Control liposome	Avanti Polar Lipids Inc (Provided by Pro.Chien Sufan from University of Louisville)	N/A
Recombinant mouse IL-23 (carrier-free)	Biolegend	Cat# 589004
Recombinant mouse IL-1β (carrier-free)	Biolegend	Cat# 575104
Recombinant mouse IL-7 (carrier-free)	Biolegend	Cat# 577802
Critical commercial assays		
TCRγ/δ+ T cell Isolation Kit, mouse	Miltenyi Biotec	Cat#130-092-125
ATP determination Kit	Invitrogen	Cat#A22066
Deposited data		
scRNA-seq data: fetal γδ T cells	Sagar et al., 2020[19]	GEO: GSE115765
scRNA-seq data: adult γδ T cells	This paper	GEO: GSE228417
Experimental models: Organisms/strains		
Mouse: C57BL/6J	The Jackson Laboratory	JAX:000664
Mouse: CD2-Cre	The Jackson Laboratory	JAX:008520
Mouse: Raptor$^{fl/fl}$	The Jackson Laboratory	JAX:013188
Mouse: Rictor$^{fl/fl}$	The Jackson Laboratory	JAX:020649
Mouse: Rorc-Cre	The Jackson Laboratory	JAX:022791
Mouse: c-Maf$^{fl/fl}$	Jun Yan laboratory	N/A

(*Continued on next page*)

Continued

REAGENT or RESOURCE	SOURCE	IDENTIFIER
Software and algorithms		
FlowJo	BD Biosciences	https://www.flowjo.com
GraphPad Prism	N/A	https://www.graphpad.com
Seurat V3	Stuart et al., 2019[64]	https://satijalab.org/seurat/
Aperio ImageScope	Leica BIOSYSTEMS	https://www.leicabiosystems.com/digital-pathology/scan/

RESOURCE AVAILABILITY

Lead contact

Further information and requests for resources and reagents should be directed to and will be fulfilled by the lead contact, Jun Yan (jun.yan@louisville.edu).

Materials availability

This study did not generate new unique reagents.

Data and code availability

Single-cell RNA-seq data have been deposited at GEO and are publicly available as of the date of publication. Accession numbers are listed in the key resources table. This paper does not report original code. Any additional information required to reanalyze the data reported in this paper is available from the lead contact upon request.

EXPERIMENTAL MODEL AND SUBJECT DETAILS

Mouse models

C57BL/6 wildtype mice were purchased from the Jackson Laboratory (Bar Harbor, ME). hCD2-Cre mice (Jackson Laboratory) were crossed with Raptor$^{fl/fl}$ mice and Rictor$^{fl/fl}$ mice (Jackson Laboratory)[28] to generate CD2-cre; Raptor$^{fl/fl}$ and CD2-cre; Rictor$^{fl/fl}$ conditional knockout (cKO) mice. c-Maf$^{fl/fl}$ mice[65] were bred with Rorc-cre mice (Jackson Laboratory) to generate control c-Maf$^{fl/fl}$ mice and Rorc-cre; c-Maf$^{fl/fl}$ cKO mice. Male and female mice were used in all experiments (embryo and infant: E16-D1, adult: 6–12 weeks old) and were housed in specific pathogen free conditions. All animals were housed and treated in accordance with institutional guidelines and approved by the Institutional Animal Care and Use Committee at the University of Louisville, Louisville, KY.

METHOD DETAILS

Cell preparation and stimulation

Thymus of pups before (E16-E20) or after birth (D1) and peripheral LNs of adult mice were grinded and filtered through 40 μm cell strainers to make single cell suspensions. Whole skin cells from mouse back skin were prepared by incubating skin tissues with digestion buffer containing collagenase IV, hyaluronidase, and DNase-I.[8] Thymocytes and peripheral lymphocytes were stimulated with phorbol myristate acetate (PMA) plus ionomycin (PMA/I) for 5h in the presence of GolgiPlug. For Mdivi-1 and Oligomycin inhibition assays, cells were treated with PMA/I for 5h in the presence of GolgiPlug in the varying concentrations of Mdivi-1 or Oligomycin. For ATP liposome assays, cells were stimulated with rmIL-23 (10 ng/ml, Biolegend) plus rmIL-1β (10 ng/ml, Biolegend) for 72h and incubated with GolgiPlug at 37°C for 5h. Intracellular IL-17/IFN-γ was measured by flow cytometry. Skin cells were stimulated with rmIL-23 (10 ng/ml, Biolegend) plus rmIL-1β (10 ng/ml, Biolegend) for 48h and incubated with GolgiPlug at 37°C for 5h, or simply incubated with GolgiPlug for 5h to test spontaneous IL-17 production.

Flow cytometry

Surface staining and intracellular staining

Fluorescent antibodies were purchased from Biolegend (CD3, γδTCR, CD4, CD8, CD27, Vγ4, Vγ5, IL-17A, IFN-γ, CD25, CD73, Thy-1.2, Anti-rat IgM), eBioscience (Fixable Viability Dye, RORγt, c-Maf, CD44, CD24), and Cell Signaling Technologies (*p*-Drp1). For cell surface marker staining, cells were first treated with Fc

Blocker and then stained with cell surface antibodies at 4°C for 20 min. The relevant isotype control antibodies were also used. For intracellular cytokine staining, cells were stained with surface antibodies followed by fixation, permeabilization (Biolegend), and finally intracellular staining of IL-17/IFN-γ at 4°C for 2h. For c-Maf/RORγt staining, cells were stained with surface antibodies (Abs), and then fixed and permeabilized with Foxp3/Transcription Factor Staining kit (eBioscience) for 45 min followed by intranuclear staining of c-Maf/RORγt at 4°C for 2h.

Phospho flow staining

For phospho-Drp1 (*p*-Drp1) flow staining, thymocytes or lymphocytes were fixed in 4% formaldehyde (Polysciences, Inc) and then permeabilized in 90% cold methanol (Fischer Chemical). Cells were stained with rabbit-*anti*-mouse *p*-Drp1 (Ser616) (Cell Signaling Technology) at 4°C overnight. On the next day, cells were washed and stained with fluorochrome-labeled donkey anti-rabbit IgG Ab, anti-mouse CD3, γδTCR and CD27 at room temperature for 30 min.

Lentivirus transduction

Primary γδ T cells were enriched from pooled lymphocytes of Rictor cKO mice by anti-mouse γδ T cell microbeads (Miltenyi Biotec). Cells were seeded in an anti-γδTCR-coated 24-well plate and cultured with rmIL-23 (10 ng/ml, Biolegend) plus rmIL-1β (10 ng/ml, Biolegend) for 4 days before viral infection. Cells were resuspended in fresh pre-warmed complete RPMI 1640 medium. GFP-tagged control or c-Maf lentivirus (Applied Biological Materials, abm) was added at a final concentration of 10 m.o.i. in the presence of 8 μg/mL polybrene (Santa Cruz). Cells were gently mixed and incubated for 20 min at room temperature, and then centrifugated for 1h at 800 g at 32°C. Cells were resuspended in fresh RPMI 1640 medium and cultured with rmIL-23 plus rmIL-1β for 30 h, and then sorted for GFP^+ γδ T cells. GFP^+γδ T cells were cultured for additional 2 days and intracellular IL-17 was examined.

scRNA-seq and data processing

Single cell suspensions were performed using LNs and spleens from C57BL/6 mice (6–8 weeks old). γδ T cells from pooled LNs and spleens were sorted and were subjected to scRNAseq analysis. Single cells were captured and barcoded cDNA libraries were constructed using the Chromium Next GEM Single Cell 3' Reagent Kit (v3.1, 10X Genomics) and the Chromium Controller, according to manufacturer's instructions. Libraries were pooled and sequenced using a 28bp x 8bp x 125bp configuration for read1 x i7 index x read2 on the Illumina NextSeq 500 with the NextSeq 500/550 150 cycle High Output Kit v2.5 (20024907).

Single cell sequencing: Gene expression profiling

Bcl files were demultiplexed into fastq files using the CellRanger software (10X Genomics, v3.1.0). The total number of sequenced reads was 264,439,643 and post normalization number of reads was 262,687,046. The reads were of good quality as determined by FastQC.[66] Gene counts were measured using CellRanger 'count', utilizing the cellranger-mm10–3.0.0 reference genome for mouse. A counts matrix was generated for each individual sample and one aggregated sample with the expected number of cells set at 5,000.

The raw count data determined by CellRanger was used as input to a custom analysis pipeline in R which uses a variety of single-cell analysis tools based on Seurat. The knee plot displays a graph showing the ranked unique molecular identifier (UMI) counts for each cell barcode for data aggregated across the three groups. Cells above the inflection point represent possible doublets while those below the knee represent background cells. Cell quality control measures were analyzed using Seurat v3,[64] and cell barcodes with the following characteristics were removed from the analysis: low counts (possible background cells) with an false discovery rate (FDR) cutoff of 0.01 from the DropletUtils[67] function 'emptyDrops', high counts (possible doublet cells) with more counts than the knee plot inflection point, mitochondrial content greater than 30% and ribosomal content greater than 40%. Genes (features) were further filtered to remove retired gene identifiers, and genes that were not expressed in at least two cells.

The expression data was normalized using SCTransform[68] where cell cycle genes, ribosomal content, and mitochondrial content were regressed. The cells were then clustered and dimension reduction was performed using UMAP.[69] Initial cluster names were assigned using a modified gene set variation analysis (GSVA)[70,71] enrichment score technique. For each of these clusters, the top marker genes were identified.

Differentially expressed genes comparing each cluster to every other cluster (all pairwise comparisons) was determined using Seurat[64] and model-based analysis of single-cell transcriptomics (MAST).[72]

Measurement of mitochondrial content

For tetramethylrhodamine methyl ester (TMRM) staining, fresh thymocytes were stained with TMRM (200 nM) at 37°C for 30min in 1 mL pre-warmed PBS. Cells were washed twice with pre-warmed PBS and then stained with cell surface Abs at 4°C for 20 min.

In vivo Mdivi-1 treatment protocol

Six-week-old C57BL/6 female mice were intraperitoneally injected with Mdivi-1 or DMSO (50 mg/kg) along with suitable carriers (5% Tween 80 and 40% PEG) starting at day 0 for 5 days. Mice were euthanized at day 6 to harvest the peripheral LNs and back skin. Cells were stimulated with PMA plus ionomycin for 5h or rmIL-23 (10 ng/ml, Biolegend) plus rmIL-1β (10 ng/ml, Biolegend) for 2 days in the presence of GolgiPlug. Intracellular IL-17/IFN-γ was measured by flow cytometry.

Establishment of skin inflammation mouse models

Imiquimod (IMQ)-induced skin inflammation mouse model was established using IMQ cream.[73] Briefly, DMSO or Mdivi-1 treated mice were applied daily with IMQ cream (5%) (Aldara; 3M Pharmaceuticals) on the shaved back for 5 consecutive days. Mice were sacrificed on day 6. Skin cell suspensions from IMQ-treated skin were stained for CD45, CD11b, Gr-1, CD3, γδTCR and intracellular IL-17. Draining lymphocytes were also stained for CD3, γδTCR and intracellular IL-17 after PMA/I stimulation plus Golgi-Plug for 5h.

Skin histology and imaging mass cytometry (IMC)

The IMQ-treated mouse skin was stored in Formalin for 24-48 h at room temperature, and then rinsed with PBS and transferred to 70% ethanol. Tissues were embedded by paraffin and sectioned for Hematoxylin and Eosin (H&E) staining and IMC. For HE staining, images were acquired at ×100 magnification using Aperio Scanoscope. Epidermal thickness was determined by measuring the average interfollicular distance under the microscope in a blinded manner.

IMC antibody staining

Antibody staining was performed using Fluidigm protocol specifically for Formalin-Fixed Paraffin-Embedded (FFPE) sections (PN 400322 A3, Fluidigm) with modifications. Briefly, 10 μm of FFPE mouse skin sections were baked in microwave at high power for 1 min and followed by 3 × 10 min of de-paraffin in xylene. Rehydrate was performed in descending grades of ethanol (100%, 95%, 80%, 70%) for 5 min each and wash slides in ultrapure millipore water for 5 min. Heat-induced antigen retrieval by using pre-heated Antigen Retrieval Buffer (abcam, ab93684) at around 96°C for 16 min and slides were washed once in warmed ultrapure millipore water and once in Dulbecco's Phosphate Buffered Saline (DPBS, Sigma, D8537) for 5 min each. Slides were blocked with 3% BSA with 0.05% Tween 20 for 1 h, followed by incubation of primary antibodies at 4°C overnight in a hydration chamber. Antibodies were purchased from Fluidigm and concentration were used for anti-Hu/Ms CD11b (EPR1344)-146Nd (91H007146) at 1:100; anti-F4/80 (D2S9R)-166Er (91H030166) at 1:100; anti-Mouse Ly-6G (1A8)-141Pr (3141008B) at 1:50. After antibody incubation, wash the slides twice in DPBS containing 0.05% Tween 20 and twice in DPBS alone, 5 min each (total four times wash). The slides with mouse skin section were stained with Intercalator-Ir (Fluidigm, 201192A) in DPBS at 1:400 for 30 min at room temperature in a hydration chamber. Wash slide with DPBS for 5 min and air-dry the slide for at least 10 min at room temperature. Slides were stored in a dust-free slide box until laser ablation.

Image acquisition and visualization

Stained slides were scanned with Epson Perfection Photo Scanner (Epson, Part B11B198011) and upload the scanned image for acquisition purposes. Three regions of interest (ROIs), around 500–1500 μM^2, were ablated at 200 Hz for each sample. MCD-files created by the CyTOF Software v7.0 was processed in MCD viewer (Fluidigm) to create pseudo-colored images for marker expression visualization.

Single cell segmentation, data conversion and data analysis

Exported imaging data from MCD Viewer was processed to generate a single-cell segmentation mask by using CellProfiler software. Software of histoCAT was used to convert the mask into fcs files and followed by further data analysis with FlowJo/Plugins software.

Cellular ATP measurement

Thymocytes harvested from Rictor cKO/Control E18 pups were stained with anti-mouse CD3 and γδTCR mAbs. γδ T cells were sorted by MoFlow high-speed sorter. Cells were rested in 96-well plate for 2h at 37°C and then lysed in native lysis buffer (Abcam) for 10 min on ice. Cells were centrifuged at 20000 g for 10 min and the supernatant was collected. ATP concentration was measured by ATP determination kit (Invitrogen) according to manufacturer's instructions.

ATP vesicle treatment

The ATP vesicles and control vesicles were made by Avanti Polar Lipids Inc (Alabaster, AL). The composition was 100 mg/mL of Soy Phosphatidylcholine (Soy PC)/1,2-dioleyl-3-trimethylammonium propane (DOTAP) (50:1), Trehalose/Soy PC (2:1), 10 mM KH_2PO_4, and 10 mM Mg-ATP.[59,60] Both liposomes were reconstituted with 1640 RPMI medium before use. Thymocytes or lymphocytes were seeded in anti CD3-coated 24-well plates and stimulated with rmIL-23 (10 ng/ml, Biolegend) plus rmIL-1β (10 ng/ml, Biolegend). The cells were then treated with ATP vesicles and control empty vesicles at indicated concentrations for 72h. GolgiPlug was added in the last 5h and cells were harvested for subsequent experiments.

QUANTIFICATION AND STATISTICAL ANALYSIS

GraphPad Prism 8.0 was used to draw statistical images and perform comparative analyses. Numbers (n) refer to the number of independent experiments or mice which were indicated in relevant figure legends. Data are presented as mean ± SEM. For animal data, data was first analyzed for normality test by D'Agostino & Pearson (n = 8–10) or Shapiro-Wilk (n = 3–7) test. Between two groups, data was tested by unpaired two-tailed t test (parametric) with Welch's correction if uneven variances existed, or Mann-Whitney U test (non-parametric). For over two groups, ordinary one-way ANOVA (parametric) was used for statistical analysis. $p < 0.05$ was considered to be statistically significant.